12-2017

Toxicity and Mitochondrial Delivery of Flavonol-Based Carbon Monoxide-Releasing Molecules

Hector Jose Esquer Heredia
Utah State University

TOXICITY AND MITOCHONDRIAL DELIVERY OF FLAVONOL-BASED CARBON MONOXIDE-RELEASING MOLECULES

by

Hector Jose Esquer Heredia

A thesis submitted in partial fulfillment
of the requirements for the degree

of

MASTER OF SCIENCE

in

Toxicology

Approved:

Abby D. Benninghoff, Ph.D. Major Professor	Jeffery Hall, Ph.D., D.V.M. Committee Member
Lisa M. Berreau, Ph.D. Committee Member	Mark R. McLellan, Ph.D. Vice President for Research and Dean of the School of Graduate Studies

UTAH STATE UNIVERSITY
Logan, Utah

2017

ABSTRACT

Toxicity and Mitochondrial Delivery of Flavonol-Based Carbon Monoxide-Releasing Molecules

by

Hector Jose Esquer Heredia, Master of Science

Utah State University, 2017

Major Professor: Dr. Abby D. Benninghoff
Department: Animal, Dairy and Veterinary Sciences

Carbon monoxide (CO) has been recently recognized as a gasotransmitter with anti-inflammatory, vasoprotective, and anti-cancer properties, but the exact biological targets of CO are still unknown. Our research group previously synthesized a class of novel and structurally modifiable flavonol-based CO-releasing molecules (CORMs). The base structure, Flav-1, is fluorescent, exhibits low cytotoxicity, and releases CO after exposure to visible light. Heme-containing proteins in mitochondria are believed to be important targets of CO. Previous reports indicate that addition of a triphenyl-phosphonium (TPP) tail allows chemical structures to target mitochondria. We hypothesized that addition of a TPP tail of two or eight carbons in length to Flav-1 (Mito-Flav-C2 or -C8) would facilitate targeting of mitochondria, and thus, localized light-induced CO release. Cytotoxicity of these TPP-appended molecules was evaluated in human umbilical vein endothelial cells (HUVEC) and lung epithelial carcinoma cells (A549) using standard cell viability assays. Evaluation of cytotoxicity using the MTT

assay revealed lower toxicity of Flav-1 in HUVECs when compared to A549 cells, but addition of the TPP tails increased apparent cytotoxicity. However, unlike the MTT assay, Flav-1 with and without tails had similar toxicity when measured in HUVECs by the lactate dehydrogenase assay. Photo-degradation experiments were performed by exposing cells to a 405 nm and/or 488 nm laser, or a bright-field source, until the fluorescence emission was undetectable. Confocal microscopy images of HUVEC and A549 cells treated with 100 μM of Mito-Flav-C2 or -C8 revealed an increase in cellular uptake, compared to Flav-1. Localization of flavonols in proximity to mitochondria of both cell lines was assessed using a confocal microscope by co-staining with Hoechst 33342 and MitoTracker Red CMXRos to visualize the nucleus and mitochondria, respectively. When A549 cells were exposed to laser light or a bright-field source, the fluorescence of Mito-Flav-C2 was lost, which indicates CO release. This work highlights the successful synthesis of the first mitochondria-targeting CORMs that enable controlled and localized release of CO to further study its physiological targets.

(97 pages)

PUBLIC ABSTRACT

Toxicity and Mitochondrial Delivery of Flavonol-Based Carbon Monoxide-Releasing Molecules

Hector Jose Esquer Heredia

Despite the reputation of carbon monoxide (CO) as a silent killer, new evidence suggests that this gaseous molecule has anti-inflammatory, anti-cancer and vasoprotective properties. Unfortunately, little is known about the role of CO in the body. However, proteins present in mitochondria are believed to be important targets. We previously synthesized a class of novel and structurally modifiable flavonol-based CO-releasing molecules (CORMs). Flavonols are commonly found in fruits and vegetables. The base structure, Flav-1, is fluorescent, exhibits low toxicity, and releases CO after exposure to visible light. Previous reports indicate that addition of a triphenylphosphonium (TPP) tail allows chemical structures to enter mitochondria. We hypothesized that addition of a TPP tail of two or eight carbons in length to Flav-1 (Mito-Flav-C2 or -C8) would facilitate targeting of mitochondria, and thus, localized light-induced CO release. Toxicity of these TPP-tailed molecules was determined in human umbilical vein endothelial cells (HUVECs) and lung epithelial carcinoma cells (A549), using standard cell viability assays. Evaluation of toxicity using the MTT assay revealed lower toxicity of Flav-1 in HUVECs compared to A549 cells, but addition of the TPP tails increased toxicity in both cell lines. However, unlike the MTT assay, Flav-1 with and without tails had similar toxicity when measured in HUVECs by the lactate dehydrogenase assay. Photo-degradation experiments were performed by exposing cells until their light emission was undetectable by using lasers in the near-UV and within the visible light spectrum. Localization of the compounds was observed using a confocal microscope by co-staining with MitoTracker Red (MTR) and Hoechst to visualize the mitochondria and nucleus, respectively. Fluorescence microscopy images of cells

treated with Mito-Flav-C2 or -C8 revealed an increase in uptake, compared to Flav-1, plus co-localization with MTR, which suggests mitochondrial localization. A549 cells exposed to laser light or a full spectrum of light lost all fluorescence of Mito-Flav-C2, which indicates CO release. This work highlights the successful synthesis of the first mitochondria targeting CORMs, and that CO release is achievable using different light sources. Moreover, these TPP-tailed CORMs will allow for controlled and localized release of CO to further study its physiological targets.

ACKNOWLEDGMENTS

I would like to thank my advisor, Dr. Abby Benninghoff, who has mentored, supported, and encouraged me throughout my studies at Utah State University. It was due to her enthusiasm and passion for science that it became clear to me what career path I wanted to follow. I also thank my committee members, Dr. Lisa Berreau and Dr. Jeffery Hall, for their support and assistance in my graduate work. I would like to thank my laboratory colleagues Sumira Phatak, Trevor Fish, Jocelyn Cuthbert, and Daphne Rodriguez for always being willing to lend a helping hand. And also, Tatiana Soboleva from the Berreau laboratory for sharing her excitement for the project by discussing the future applications of it.

I am especially grateful to Dr. Lisa Berreau and Dr. Abby Benninghoff for giving me the opportunity to work in their lab as an inexperienced undergraduate research assistant, which helped me discover my passion for scientific research.

This work was supported by the Ministry of Superior Education, Science, and Technology of Dominican Republic, the Utah Agriculture Experiment Station (project number UTA-01178) and a USU Office of Research and Graduate Studies, Research Catalyst grant.

Hector Esquer

CONTENTS

Page

LIST OF TABLES

LIST OF FIGURES

LIST OF ABBREVIATIONS AND SYMBOLS

Abbreviations

A549	Lung adenocarcinoma cells
ACN	Acetonitrile
ATCC	American type culture collection
ATP	Adenosine triphosphate
BP	Band pass
CO	Carbon monoxide
COHb	Carboxyhemoglobin
COP-1	Carbon monoxide probe-1
CORM	Carbon monoxide-releasing molecule
COX	Cytochrome c oxidase
DMEM	Dulbecco's modified Eagle's medium
DMF	N,N-Dimethylformamide
DMSO	Dimethyl sulfoxide
EDC	1-ethyl-3-(3-dimethylaminopropyl)carbodiimide hydrochloride
EDTA	Ethylenediaminetetraacetic acid
ET-CORM	Enzyme-triggered carbon monoxide-releasing molecule
ETC	Electron transport chain
EtOH	Ethanol
F-12K	Ham's F-12K (Kaighn's medium)
FBS	Fetal bovine serum
FCCP	Carbonyl cyanide-p-trifluoromethoxyphenylhydrazone
HOBt	Hydroxybenzotriazole
HCT116	Human colorectal carcinoma cells
HeLa	Human cervical cancer cells
HepG2	Human hepatoma cells
HO	Heme oxygenase
HUVEC	Human umbilical vein endothelial cell
IC_{50}	Half-maximal inhibitory concentration
Irr	Irradiated
KG1	Human macrophage cells
LDH	Lactate dehydrogenase
LLC-PK1	Porcine kidney epithelial cells
LSM	Laser scanning microscope
MTR	MitoTracker Red CMXRos
MTT	(3-(4,5-dimethylthiazol-2-yl)-2,5-diphenyltetrazolium bromide
ND	No significant decrease
O_2	Molecular oxygen/dioxygen
PBS	Phosphate buffered solution
pH	Potential of hydrogen
PhotoCORM	Photo-induced carbon monoxide releasing molecule
PTEC	Human proximal tubular epithelial cells

RAW 264.7	Murine macrophage cells
ROS	Reactive oxygen species
SEM	Standard error of measurement
TNF	Tumor necrosis factor
TPP	Triphenylphosphonium
UV	Ultraviolet

Symbols

cm	Centimeter
h	Hour
µm	Micrometer
M	Molar
mg	Milligram
min	Minute
ml	Milliliter
mm	Millimeter
mol	Mole
nm	Nanometer
nM	Nanomolar
U	Unit
v/v	volume/volume
µL	Microliter
µM	Micromolar

INTRODUCTION

Carbon monoxide (CO) may have the potential to become a future therapeutic, despite its reputation as a killer gas. CO is a colorless, tasteless, odorless, and toxic gaseous molecule. Briefly, CO is toxic due to its high binding affinity to heme-containing proteins such as hemoglobin. CO binding to hemoglobin disrupts the oxygen carrying capacity of this important transport protein and renders it unable to deliver oxygen to tissues within the body. Therefore, high concentrations (5,000 ppm for 5 min) or prolonged exposure to CO (1,500 ppm for more than 1 h) can lead to systemic hypoxia, unconsciousness, and even death according to the National Institute for Occupational Safety and Health (NIOSH) (1994).

In the late 1940s, Sjöstrand *et al*. (1949) observed that physiological decomposition of hemoglobin *in vivo* produced CO. Later, Tenhunen and colleagues (1968) determined that heme oxygenase (HO) enzymes were responsible for the degradation of heme groups to produce CO, free iron, and biliverdin. These discoveries led researchers to suspect possible physiological roles for endogenous CO. Several groups have already elucidated the anti-inflammatory, (Chapman *et al.*, 2001; Motterlini, 2007; Mu *et al.*, 2014; Otterbein *et al.*, 2000; Takagi *et al.*, 2011) vaso-protective, (Kim *et al.*, 2015; Motterlini, 2007; Ndisang *et al.*, 2004; Yang *et al.*, 2014) and anti-apoptotic properties (Al-Owais *et al.*, 2015; Brouard *et al.*, 2000) of CO. Additionally, researchers have uncovered the capacity of CO to induce mitochondrial biogenesis, which may modulate cellular metabolism (Almeida *et al.*, 2015; Suliman and Piantadosi, 2014; Wang *et al.*, 2016). Notably, these beneficial effects are observed at low concentrations of CO. Therapeutic concentrations of CO gas range from 50 to 1000 ppm

for up to 1 h in rats or mice, with 250 ppm being the most frequently used concentration of CO (Motterlini and Otterbein, 2010). Although these concentrations of inhaled CO are known to elicit beneficial effects, the exact concentration that accumulates inside the cell is still unknown (Motterlini and Foresti, 2017). The lack of knowledge of exact intracellular concentrations of CO also holds true for other delivery methods, as discussed below.

Given such important physiological effects, studies involving the relationship between HO and its enzymatic byproduct CO have inspired the development of technologies that take advantage of these intricate pathways. Early experiments assessed the effects of CO via inhalation or by overexpression or induction of HO-1 (Brouard, *et al.*, 2000; Otterbein, *et al.*, 2000; Sato *et al.*, 2001), which is the inducible isoform of three distinct HOs. Although administration of exogenous CO through inhalation has remained a viable option for research due to its relative simplicity, several drawbacks can be noted. Example disadvantages include the poor reliability of using carboxyhemoglobin (COHb) as a marker of exposure to CO and whether exposure to CO at low concentration dosage intervals is more effective than a high single dosing (Motterlini and Otterbein, 2010). Moreover, it remains unclear if a localized tissue exposure to CO would increase efficacy of delivery to cellular targets since distribution of the gaseous molecule after inhalation is dependent on the partition ratio between the different tissues and body fluids (Schatzschneider, 2015). In addition, CO administered by inhalation may require hospital visits and proper equipment handling by trained personnel, which can prove difficult for continuous treatments. Despite these

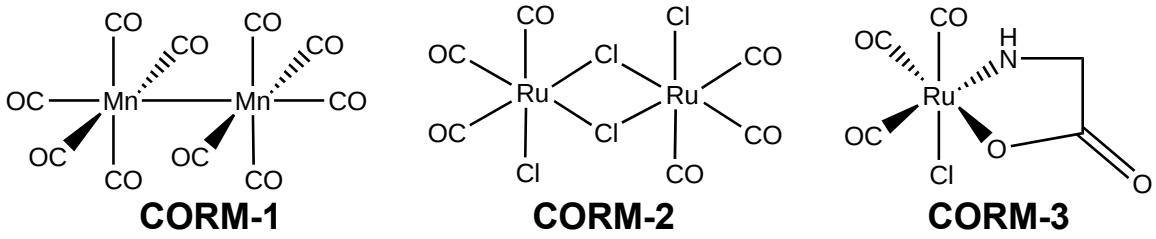

Figure 1. Chemical structures of first-generation CO-releasing molecules.

disadvantages, a promising CO delivery system has been developed. Covox DS is a device developed by Ikaria that delivers CO gas in proportion to the patient's body weight and is independent of the patient's respiration rate (Motterlini and Otterbein, 2010). Briefly, the device is adjusted to deliver CO gas at a mg per hour rate and releases CO at the beginning of each inspiration.

For the reasons outlined above, the study of the therapeutic effects of CO may require a safer and, perhaps, a more conventional drug-like approach. Thus, CO-releasing molecules (CORMs) were developed to help localize the interaction of CO with physiological targets and to decrease the amount of non-specific binding to hemoglobin and myoglobin that occurs from inhaled CO (Motterlini and Foresti, 2017). Therefore, CORMs may reduce the concentrations of CO required to produce the same physiological effects as inhaled CO. Most CORM structures, including early iterations, are based on metal-carbonyl complexes, which release CO upon ligand exchange (Figure 1; Table 1). The first CORM, named CORM-1, contains manganese, requires UV-light to release CO, and is insoluble in water (Mann, 2012). The second and third CORMs, CORM-2 and CORM-3, replaced manganese with ruthenium and are soluble in DMSO and water, respectively. These two important CORMs have been extensively utilized with more than 200 published papers describing their use, to date (reviewed in Mann, 2012).

Table 1. Summary of the Properties of Example CO-Releasing Molecules (CORMs)

Name	CO-release trigger	Metal Center	Classification	Fluorescence emission	Solubility
CORM-1[a]	UV-light	Fe	PhotoCORM	No	Organic solvents
CORM-2[a]	Interaction with heme-proteins	Ru	Ligand exchange	No	Organic solvents
CORM-3[a]	Solution chemistry	Ru	Ligand exchange	No	Aqueous solutions
CORM-A1[a]	Solution chemistry	B	Ligand exchange	No	Aqueous solutions
CORM-401[b]	Solution chemistry	Mn	Ligand exchange	No	Organic solvents
ALF785[c]	Solution chemistry	Mo	Ligand exchange	No	Aqueous solutions
BW-CO-101[d]	Solution chemistry	None	Ligand exchange	Product only	Organic solvents
rac-1[e]	Esterases	Fe	Enzyme triggered-CORM	No	Aqueous solutions
rac-8[e]	Esterases	Fe	Enzyme triggered-CORM	No	Aqueous solutions
BW-ETCO-101[d]	Esterases	None	Enzyme triggered-CORM	No	Organic solvents
Diketone derivative[f]	Visible light	None	PhotoCORM	Yes	Micelles
Xanthene-9-carboxylic acid[g]	Visible light	None	PhotoCORM	Yes	Aqueous solutions
BODIPY derivative[h]	Visible light	None	PhotoCORM	Yes	Aqueous solution
Flav-1[i]	Visible light	None	PhotoCORM	Yes	Organic solvents

[a] (Motterlini, 2007)
[b] (Vummaleti *et al.*, 2012)
[c] (Marques *et al.*, 2012)
[d] (Ji *et al.*, 2017)
[e] (Romanski *et al.*, 2013)
[f] (Peng *et al.*, 2013)
[h] (Palao *et al.*, 2016)
[g] (Antony *et al.*, 2013)
[i] (Anderson, *et al.*, 2015)

Furthermore, experiments using these compounds were able to mimic the effects of CO inhalation and upregulation of HO-1 expression (Otterbein *et al.,* 2016), making them attractive alternatives for CO delivery. However, CORM-3 releases CO in solution very rapidly ($t_{½}$<1 min). A very short half-life, the presence of several isomeric forms, and a variable rate of CO release limit the applications of CORM-3 (Johnson *et al.*, 2007; Mann, 2012; Motterlini and Otterbein, 2010).

Therefore, to explore other desirable features, available CORMs were modified or new CORMs were synthesized. These modified or new molecules replaced ruthenium with different metals, such as iron, cobalt, iridium, rhenium, tungsten, molybdenum, and chromium. New and modified CORMs enabled tuning of the rate of CO release and increased cellular uptake of the compounds (Kautz *et al.*, 2016; Schatzschneider, 2015). Figure 2 shows the chemical structure of several later generations of ligand exchange CORMs. CORM-401 is able to release three CO molecules per mole of compound at pH 7.4 and 37 °C. Interestingly, the reaction appears to be reversible by recapturing released CO. However, in the presence of a CO target, such as myoglobin, the reversible reaction is prevented, which may suggest some targeting capacity (Crook *et al.*, 2011). A notable non-metal example is CORM-A1, which contains boron. At physiological conditions, CORM-A1 has a 21 min half-life for CO release (Figure 2). Dr. Wang and colleagues (2014) developed a click chemistry approach to synthesize metal-free CO-releasing pro drugs. Expanding on their previous work, Wang and group were able to improve the previous click chemistry design to a more structurally modifiable intramolecular CO-releasing pro drug, BW-CO-101 (Ji *et al.*, 2016). On the other hand, Marques *et al.*

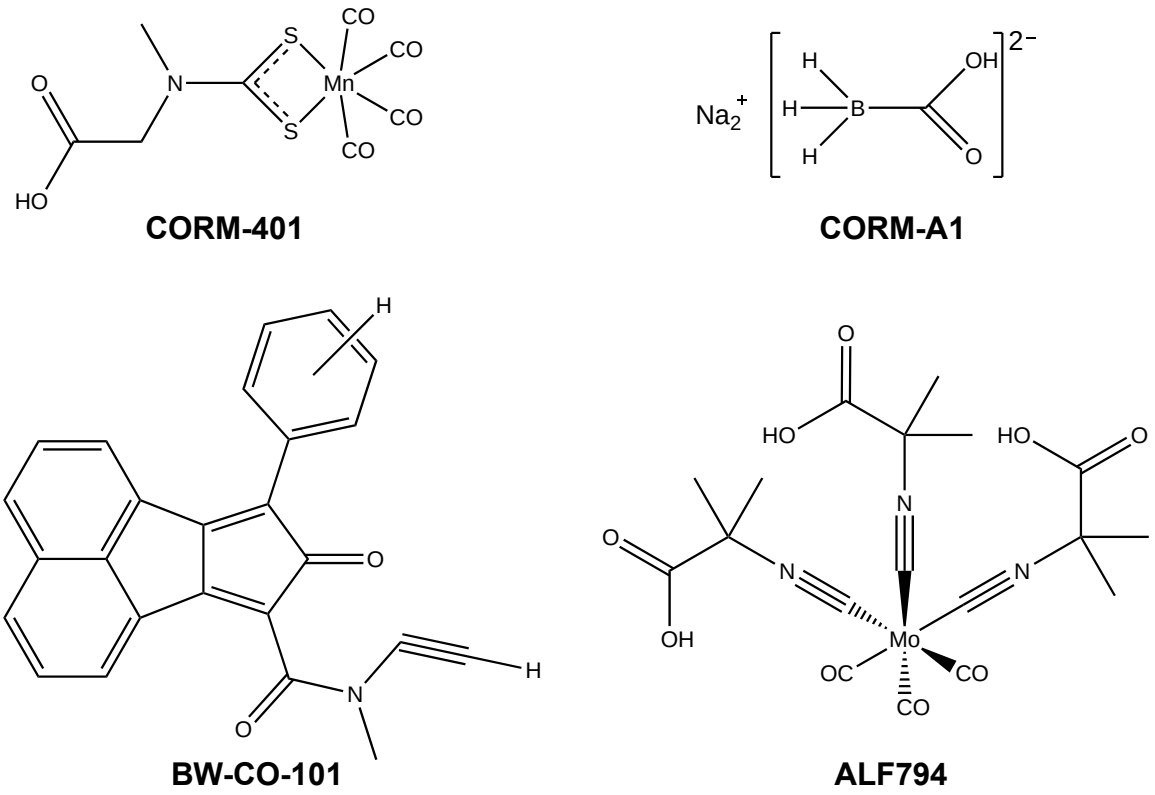

Figure 2. Chemical structures of example CORMs that operate via a ligand-exchange mechanism.

(2012) developed molybdenum-containing CORMs, such as ALF794 (Figure 2), aimed to deliver CO in a targeted manner to the liver. ALF794 efficiently elevated CO concentrations in the liver, whereas removal of the methyl substituents on this structure (illustrated by molecule ALF795) enhanced protection of the liver *in vivo* in the acetaminophen-induced liver injury mouse model.

When designing experiments, investigators must consider that the metal-containing fragments remaining after CO release may produce unknown biological interactions (Schatzschneider, 2015). The presence of free metals could catalyze Fenton reactions (Mann, 2012), which are a source of reactive oxygen species (ROS). Ideally,

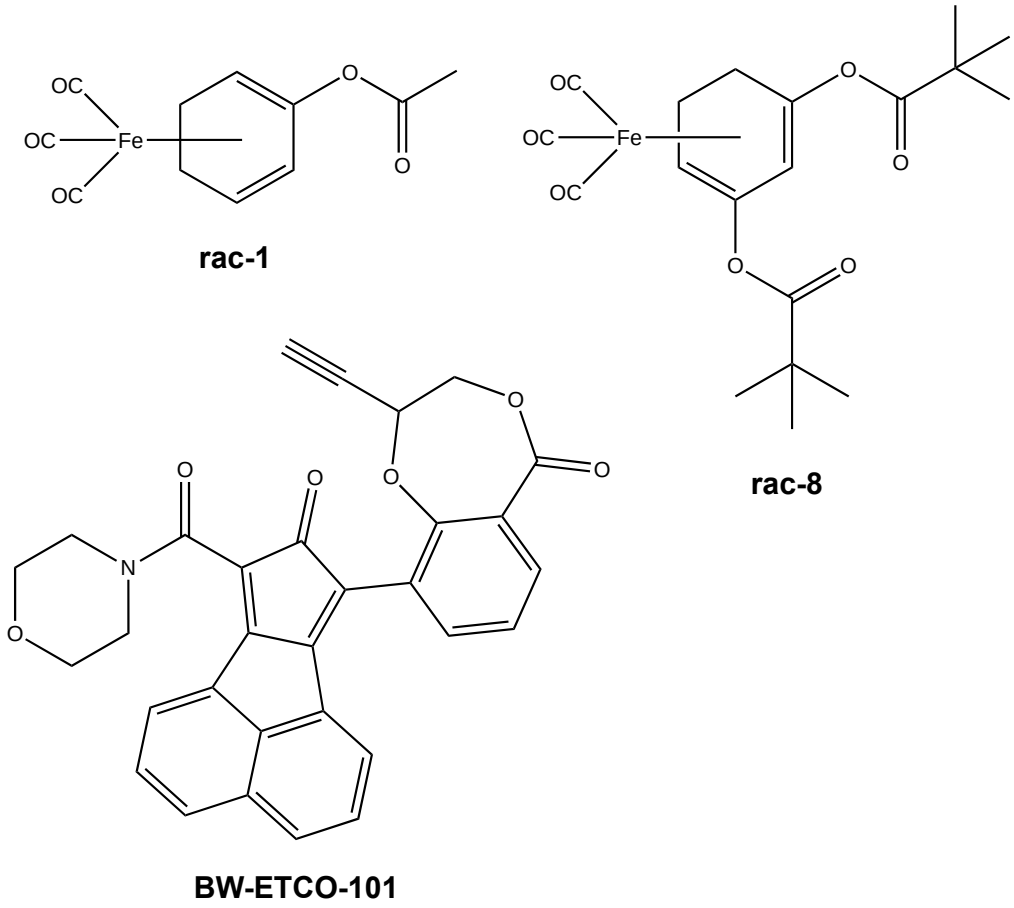

Figure 3. Chemical structures of CORMs that operate via an enzyme-triggered mechanism.

CORMs will be administered as oral drugs that can release CO systemically at established rates or be targeted to specific locations in cells or in the body. In addition, CORMs may benefit substantially by controllable CO release trigger mechanisms, such as enzymatic catalysis (ET-CORMs), photolysis (photoCORMs), and even magnetic heating (Kautz, *et al.*, 2016).

The ability to trigger CO release from ET- or photoCORMs allows for precise spatial and/or temporal control of the release of CO. However, concentrations of intracellular CO release may be limited by the presence of extracellular esterases *in vivo*

(Jobsis *et al.*, 2007). Romanski *et al*. (2013) measured *in vitro* the protective effects of rac-1, an ET-CORM, and its derivatives (Figure 3) on hypothermia-associated cell damage, and noted that structural modifications modulated the CO-associated protective effect. The compounds were modified by shifting the double bonds present in the ring structure into an inner or outer position with respect to the ester, along with various substituent combinations. The variability of biological activity of these compounds among cell lines can be detrimental to their development as a therapeutic agent. However, these differences can be beneficial if ET-CORMs are developed to target specific cell lines and to produce specific biological activities and not others. Adding to the ET-CORM field, Ji *et al.* (2017) modified their click chemistry CO-releasing pro drugs to include esterase-catalyzed CO release, as illustrated by the molecule BW-ETCO-101 (Figure 3). Importantly, ET-CORMs may be modified to include other enzymatic systems, such as proteases or decarboxylases, or a higher affinity to specific esterases present in target cells.

The first CORM structure developed, CORM-1, is a photoCORM that requires exposure to UV-light for CO release (Mann, 2012). Like ET-CORMs, photoCORMs provide an attractive mechanism for CO release. Whereas ET-CORMs only allow for spatial control, photoCORMs provide for both spatial and temporal control. At the time this work was initiated, most photoCORM structures required near UV-light to undergo CO release, making them difficult to be used as future therapeutics because of the potential for UV-induced cell damage. The use of lower energy wavelengths for photolysis is an important aspect of photoCORM development because it reduces the

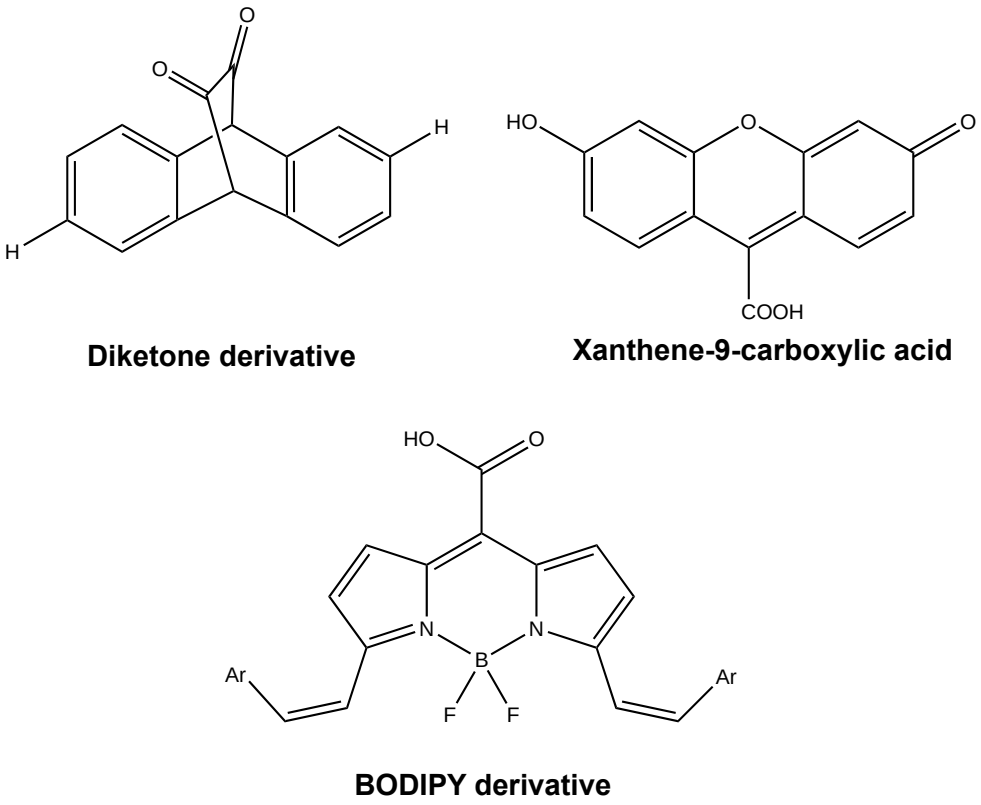

Figure 4. Chemical structures of CORMs that operate via a light-induced mechanism.

damage caused by UV-light to cells, while also allowing for deeper penetration of light into tissue. Importantly, Chakraborty *et al*. (2014a; 2014b) showed that different ligand/coligand combinations on metal-coordinated systems can lower the energy of light required for and the rate of CO release. Notably, only a few metal-free photoCORMs have been synthesized, including 1) a xanthene-9-carboxylic acid, which releases CO when exposed to 500 nm light at a pH range of 5.7-7.4 in aqueous solution (Antony, *et al.*, 2013); 2) a micelle-encapsulated diketone derivative (Figure 4), which releases two equivalents of CO when irradiated at 470 nm (Peng, *et al.*, 2013); 3) boron-dipyrromethene (BODIPY) derivatives (Figure 4) capable of releasing CO when exposed

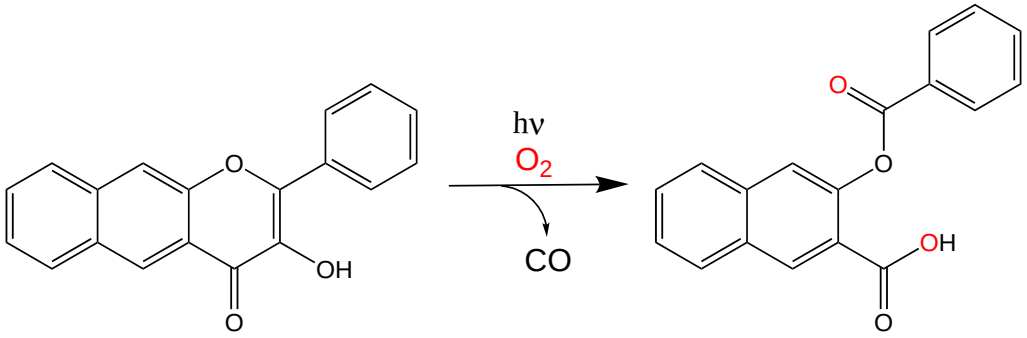

Flav-1 **Irr-Flav-1**

Figure 5. Reactivity of Flav-1 in the presence of 419 nm light (in DMSO) and O_2. This reaction generates free CO and the light irradiated product of Flav-1 (Irr-Flav-1). (Anderson *et al.*, 2015)

to visible and near infrared light (300-730 nm) (Palao, *et al.*, 2016); and 4) a structurally-tunable flavonol derivative (Flav-1) that releases CO (Figure 5) when exposed to 419 nm light and in the presence of oxygen (Anderson, *et al.*, 2015).

The work presented in this thesis was performed on flavonol-based photoCORMs developed by Dr. Berreau and colleagues (Anderson, *et al.*, 2015). Flavonoid compounds are commonly found in fruits, vegetables, and seeds and are known to have anti-oxidant and free-radical scavenging activities (Chahar *et al.*, 2011). The core structure of Flav-1 represents a new class of metal-free photoCORMs. Notably, Flav-1 has several important features that are relevant in the field of CORMs. First, Flav-1 is excitable with blue light (BP 470/40 filter) in cell culture media and has detectable emission using a standard green fluorescent protein filter (BP 525/50 filter) (Figures 6 and 7). Second, Flav-1 is stable and soluble in media supplemented with 10% fetal bovine serum (FBS) at 37 °C and pH of 7.4. Third, the photoreaction releases one CO equivalent and results in the loss of the fluorescence emission characteristic of Flav-1. The photodegradation of

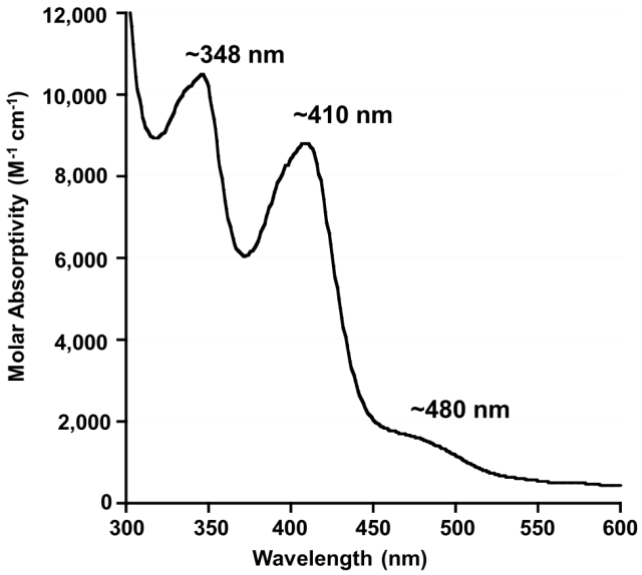

Figure 6. Absorption spectrum of Flav-1. Flav-1 was solubilized in DMEM-F12 media supplemented with 10% FBS 100 µM. Data shown with permission of collaborators Tatiana Soboleva and Lisa Berreau, Utah State University.

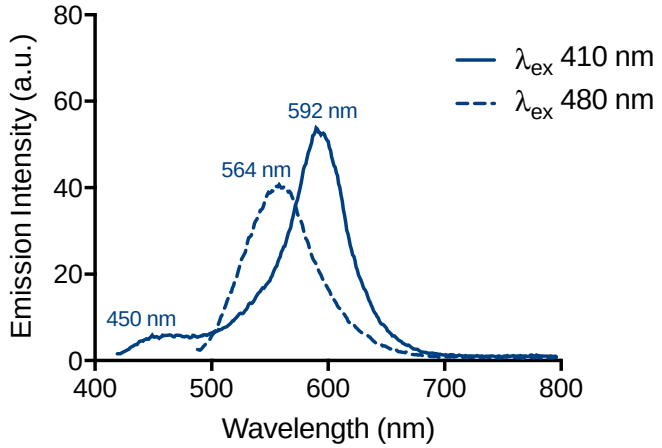

Figure 7. Emission spectra of Flav-1. Flav-1 was solubilized in DMEM-F12 media supplemented with 10% FBS to a concentration of 100 µM and exposed to 410 nm (solid line) or 480 nm (dashed line) excitation light. Data shown with permission of collaborators Tatiana Soboleva and Lisa Berreau, Utah State University.

Flav-1 yields a single, characterized, non-toxic product, Irr-Flav-1 (Figure 5). Recently, Popova and colleagues (2017) determined that Flav-1 is stabilized in part to its anionic form when solubilized in 1:1 DMSO:PBS at pH 7.4. This stabilization of the anionic form red-shifts the absorption maximum of Flav-1 and its emission wavelengths compared to being solubilized in acetonitrile. Furthermore, Figure 6 shows evidence of the presence of the anionic form of Flav-1 in media supplemented with FBS, as indicated by the observed spectral band at approximately 480 nm. Thus, the anionic form of Flav-1 in media allows for CO release at higher wavelengths of light compared to other solutions.

The structural tunability of Flav-1 has allowed us to explore modifications that could increase cellular uptake or target the molecule to specific organelles. Due to the important roles of mitochondria in cellular metabolism and cell survival, a number of molecules have been targeted to these important organelles. A successful approach to localize molecules to the mitochondria has been the use of a triphenylphosphonium (TPP) cation moiety (Figure 8). This structural motif allows molecules to cross lipid bilayers and to accumulate in the mitochondria driven by a large electric potential (Zielonka *et al.*, 2017). For example, by attaching a TPP cation moiety to the active phenolic group of vitamin E (MitoE2), Smith, *et al*. (1999) showed that the modified antioxidant was able to protect the mitochondria from oxidative damage by decreasing both lipid peroxidation and protein damage (Figure 8). Also, several other antioxidant compounds have been used as possible mitochondria-targeting therapeutics, such as MitoSOD, MitoPeroxidase, MitoQ10, and MitoTEMPOL (Figure 8) (Murphy and Smith, 2007). MitoQ10 has been

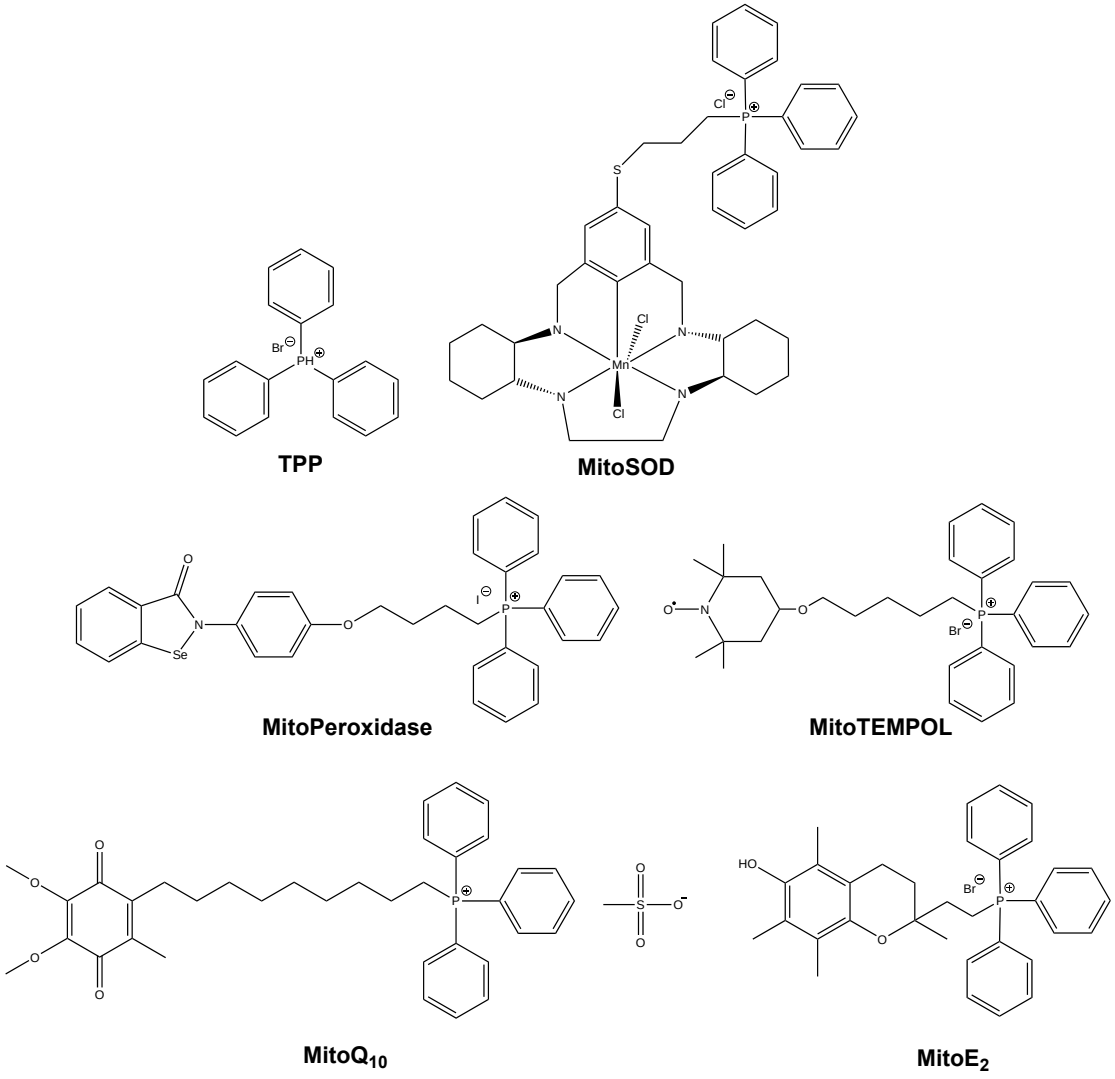

Figure 8. Chemical structures of the TPP motif and several available TPP-appended compounds.

shown to protect against the development of hypertension, improve endothelial function, and reduce cardiac hypertrophy (Graham *et al.*, 2009).

As previously stated, mitochondria maintain proper metabolic control in cells. These organelles are not only the major site of ATP production, but they coordinate other critical metabolic pathways through the Krebs cycle, fatty acid metabolism, cell

proliferation, inflammatory and anti-inflammatory pathways, and cell viability (Suliman and Piantadosi, 2014). Although experiments have elucidated the beneficial effects of low amounts of CO *in vivo*, a mechanistic understanding is lacking. Mitochondria have been proposed to be the target organelle for CO-induced biological effects. For example, cytochrome c oxidase (COX), also known as Complex IV, is a known binding target for CO. However, various studies have yielded contrasting results with respect to COX-specific activity (Almeida *et al.*, 2012; Queiroga *et al.*, 2011; Zuckerbraun *et al.*, 2007). For example, Almeida and colleagues (2012) observed an induction of COX activity in isolated mitochondria of primary astrocytes when treated with 10 μM of CO. Meanwhile, Queiroga *et al.* (2011) observed a transient effect on COX activity of liver mitochondria treated with 10 μM CO. Briefly, after 10 min, COX activity was prevented, while 30 minutes after exposure COX activity was slightly increased. Finally, Zuckerbraun and colleagues (2007) observed a decrease in COX activity after exposure to 250 ppm (8.9 mM) of CO in permeabilized RAW 264.7 cells. These differences might be explained by the different concentrations tested, periods of exposure, and time points in which COX activity was measured (Queiroga *et al.*, 2012), and in Zuckerbraun's experiment, the use of whole cells as opposed to isolated mitochondria. Interestingly, the rate of mitochondrial respiration appears to be modulated when treated with CORM-3, and it can be increased or decreased depending on the treatment concentration, ranging from 0.5-50 μM (0.14-1.4 ppm) (Lancel *et al.*, 2009). Although the experiments performed by these scientists showed important biological effects attributed to CO, it remains a challenge to compare their results in a systematic manner. Thus, a current

limitation in the field of CO is the development of a unifying delivery method that can localize in the biological compartments of interest.

In addition to COX activity, mitochondrial biogenesis, an increase in number of mitochondria, seems to play a major role in the biological effects produced by CO. Therefore, COX activity, mitochondrial respiration, and mitochondrial biogenesis appear to be linked in the improvement of metabolism and energetic status on the mitochondria (Almeida, *et al.*, 2015; Lancel, *et al.*, 2009; Queiroga, *et al.*, 2012; Suliman *et al.*, 2007; Suliman and Piantadosi, 2014; Suliman and Piantadosi, 2016; Wang, *et al.*, 2016). A recent paper by Sun and colleagues (2017) showed that CO treatment attenuated oxidative stress triggered by oxidized low density lipoproteins. Briefly, human umbilical vein endothelial cells (HUVECs) were treated with 5-50 μM of CORM-2, and then cell viability was assessed. They observed a decrease in cell death triggered by oxidative stress when cells were treated with 20 and 50 μM of CORM-2. CORM-2 suppressed cytochrome c release from the mitochondria, inhibited the mitochondrial permeability transition pore, and inhibited the Wnt/β-catenin pathway. These apparent molecular responses to CORM-2 are all known to modulate cell apoptosis.

Until recently, most CORMs released CO spontaneously upon solubilization, which limited their ability to release CO within specific tissues or organs. Scientists noted the limitations of this model and implemented different methods of CO-delivery. In addition to the previously mentioned ET-CORMs and photoCORMs, other modified CORMs have been designed. Kautz *et al*. (2016) described these modifications as CORM conjugates, which involve the use of peptides, polymers, micelles, nanoparticles,

dendrimers, biocompatible metal-organic frameworks, and self-assembled protein cages to accumulate the compounds into different tissues. These conjugated CORM structures aimed to reduce cytotoxicity of the parent compound, enhance permeability and retention, and extend the half-life of the CO release reaction to facilitate intracellular CO delivery. However, to our knowledge, none of these conjugates facilitated delivery of the CORM to specific cellular organelles.

To fully understand the mechanistic effects of CO, the field would be advanced by mitochondria-targeting CORMs that enabled more precise study of physiological targets of this gaseous molecule. Therefore, our objective was to use the structurally-tunable framework of Flav-1 (Anderson, *et al.*, 2015) to design CORM structures that target mitochondria, thus facilitating delivery of CO to this organelle in a manner under both spatial and temporal control. We hypothesized that modification of the Flav-1 structure by addition of a TPP tail moiety of varying lengths (2 and 8 carbons) would facilitate targeting of this CORM, and thus CO release, to the mitochondria. Additional specific objectives were to assess the cytotoxicity of these modified compounds using HUVEC and A549 cell models and confirm their mitochondrial targeting capability via confocal microscopy.

MATERIALS AND METHODS

Synthesis of targeting compounds. Synthesis of photoCORMs to target the mitochondria was performed by members of the Berreau laboratory at Utah State University. Mito-Flav-C2 (2 carbon tail length) was synthesized according to the scheme depicted in Figure 9. A separate preparation of the TPP tail and flavonol was required before their coupling. Hence, the TPP tail was synthesized in a one-step reaction between 2-bromoethylamine hydrobromide and triphenylphosphine. Flav-1 (3-hydroxy-2-phenyl-benzo[*g*]chromen-4-one) was synthesized as previously described (Anderson, *et al.*, 2015), but using a *p*-carboxy-benzaldehyde. The obtained tail and flavonol were subsequently coupled to form Mito-Flav-C2 with a final yield of 68%. The purified product was characterized by NMR spectroscopy and mass spectroscopy to confirm the structure, and the experimental results were in good agreement with the theoretical values (Figure A1). Absorption and emission spectra for Mito-Flav-C2 are also provided in the appendix (Figures A2-A4).

Mito-Flav-C8 was synthesized as detailed in Figures 10-11. A separate preparation of tail and flavonol was necessary before their coupling. Hence, the tail was synthesized in a five-step reaction pathway (Figure 10). Initially, 1,8-octanediol was brominated to yield 8-bromo-1-octanol, which was subsequently combined with phthalimide to obtain 2-(8-hydroxyoctyl)-1H-isoindole-1,3(2H)-dione. The latter was mixed with hydrazine monohydrate to give 8-amino-1-octanol that was further brominated to give 8-amino-1-bromooctane hydrobromide salt. The obtained salt was refluxed with triphenylphosphine to yield C8-TPP. The obtained tail and flavonol were

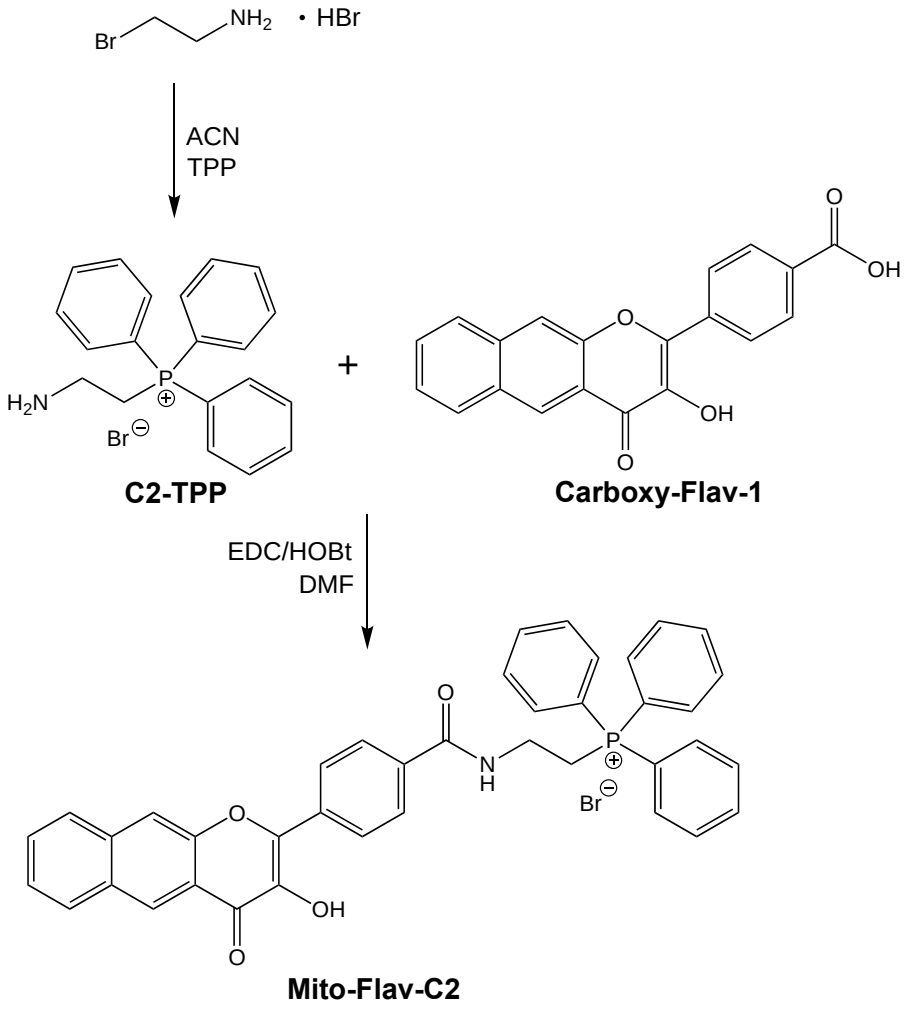

Figure 9. Scheme depicting synthesis of Mito-Flav-C2 (two carbon length TPP-tail). TPP, triphenylphosphine; C2-TPP, two-carbon length TPP-tail; ACN, acetonitrile; EDC, 1-Ethyl-3-(3-dimethylaminopropyl) carbodiimide; HOBt, hydroxybenzotriazole; DMF, dimethylformamide.

subsequently coupled to form Mito-Flav-C8 with a final yield of 62% (Figure 11). The purified product was characterized by NMR spectroscopy and mass spectroscopy to confirm the structure, and the experimental results were in good agreement with the theoretical values (Figure A5). Emission and absorption spectra for Mito-Flav-C8 are also provided in the appendix (Figures A6-A8).

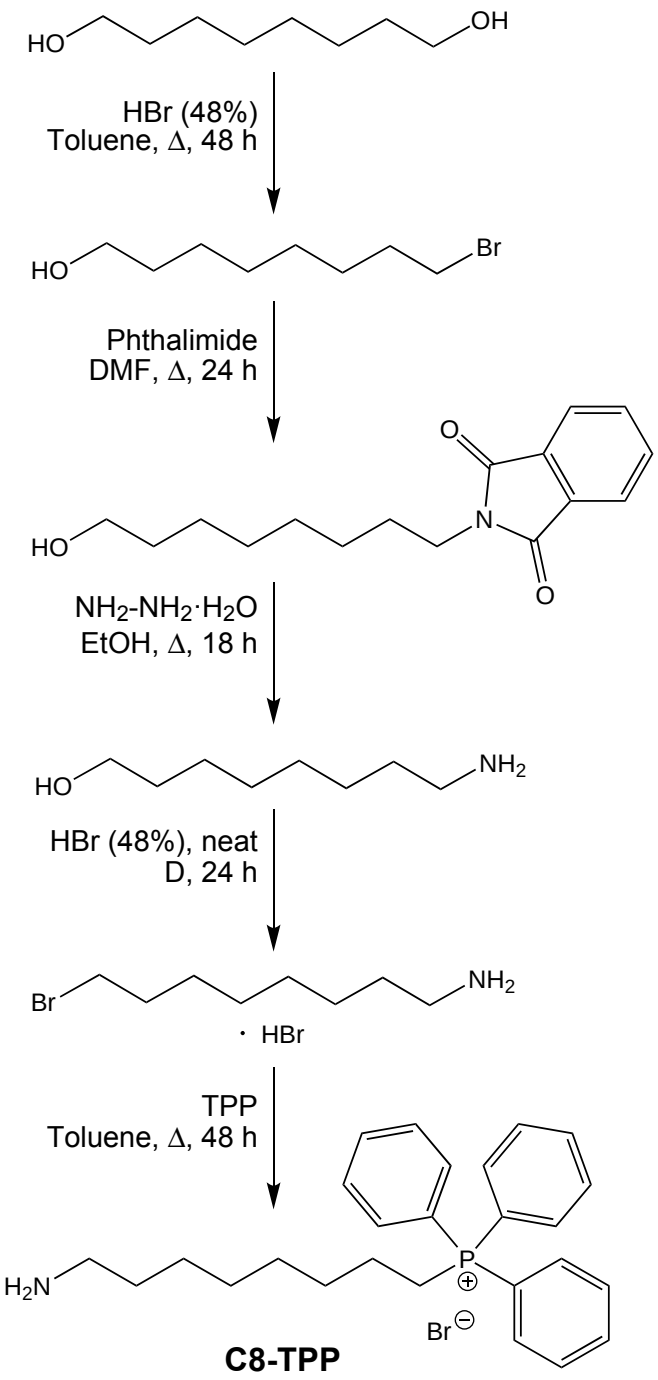

Figure 10. Scheme depicting synthesis of eight-carbon triphenylphosphine (C8-TPP)-appended tail. HBr, hydrogen bromide; DMF, dimethylformamide; EtOH, ethanol.

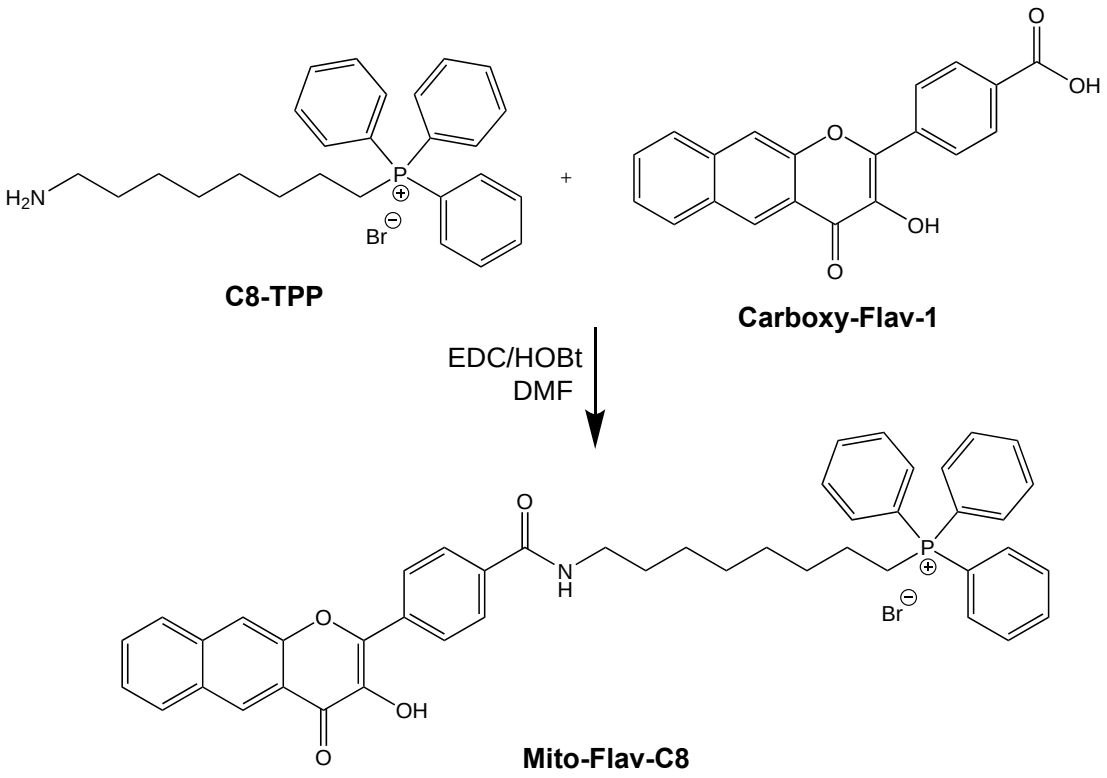

Figure 11. Scheme depicting synthesis of Mito-Flav-C8 using carboxy-Flav-1 and an eight-carbon triphenylphosphine tail (C8-TPP). EDC, 1-Ethyl-3-(3-dimethylaminopropyl) carbodiimide; HOBt, hydroxybenzotriazole; DMF, dimethylformamide.

Absorption and emission spectra of flavonol-based compounds. To determine the appropriate excitation wavelength for the flavonol-based compounds for confocal experiments, absorption spectra of all compounds at 100 µM were measured using a Varian Cary® 50Bio spectrophotometer (Agilent Technologies, Santa Clara, CA) at 37 °C, in media prepared with 10% (v/v) FBS (Caisson Laboratories, Logan, UT) and without FBS in a cell-free system. The absorbance profiles for these TPP-appended photoCORMs were different in the presence of FBS, noted by the additional absorption feature at 480 nm (Figures A4 and A8). The presence of this absorption feature allowed

for the illumination of the photoCORMs well within the visible light range for subsequent *in vitro* experiments described below. Light emission intensity was measured using a Shimadzu RF-530XPC spectrometer in the range of 295-800 nm by exciting the compounds at two different wavelengths, 410 and 480 nm, to reproduce as closely as possible the lasers on the confocal microscope to be used (405 and 488 nm) (Figure 12). During the preparation of stock solutions of Flav-1 and the TPP-appended compounds for spectroscopic analyses, it was noted that the compounds tended to precipitate when solubilized in aqueous solution or culture media without the presence of FBS. This observation suggested that the photoCORMs may adhere or otherwise interact with serum proteins in FBS, resulting in reduced free compounds in the media. Thus, when considering the concentrations for *in vitro* experiments described below, the concentration specified is the nominal concentration that does not account for potential

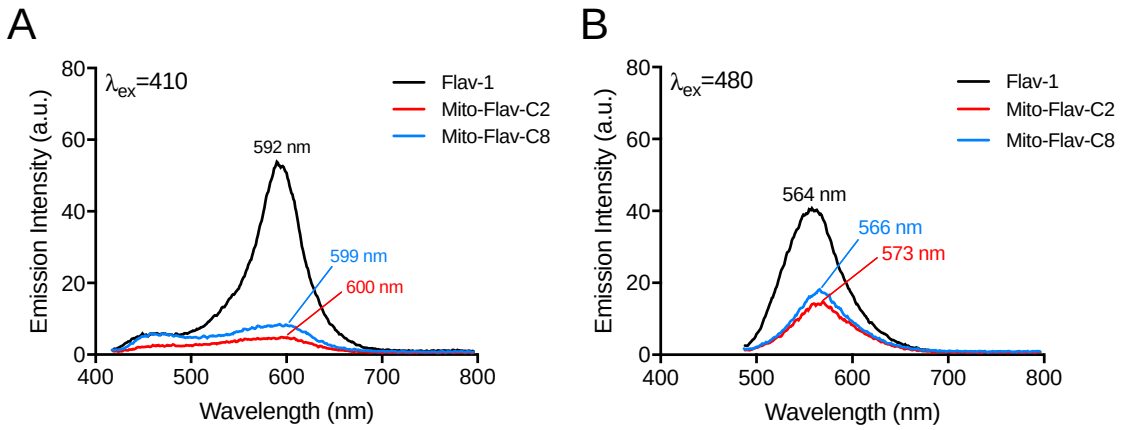

Figure 12. Emission intensity spectra for Flav-1, Mito-Flav-C2, and Mito-Flav-C8. Spectra were obtained for each CORM at 100 μM in DMEM F12 media with 10% FBS after excitation at 410 nm (A) or 480 nm (B). Approximate wavelengths for maximum emission intensities are shown. Data shown with permission of collaborators Tatiana Soboleva and Lisa Berreau, Utah State University.

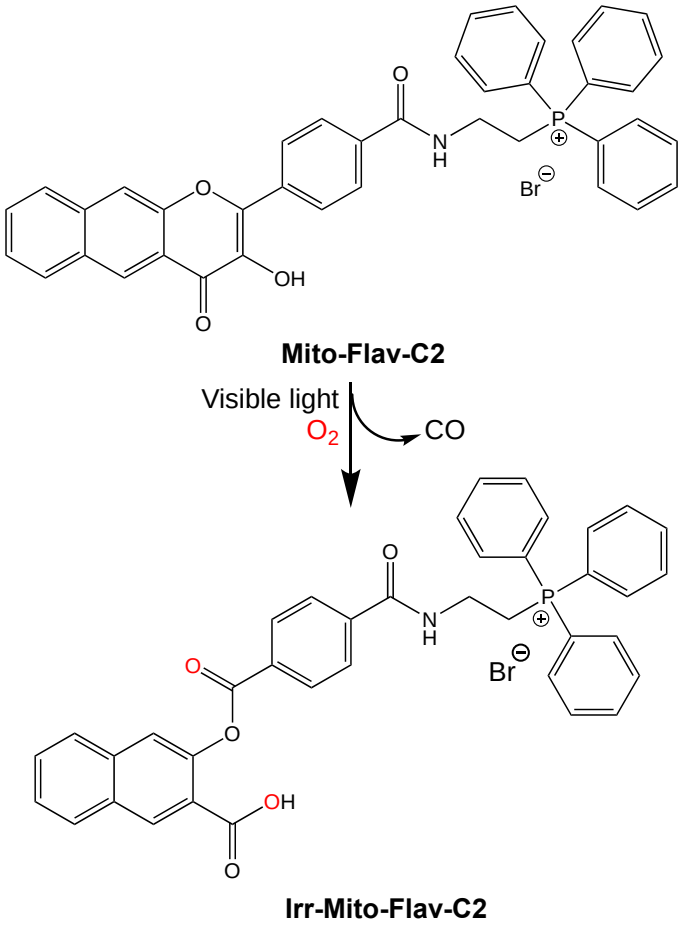

Figure 13. Photodegradation reaction of Mito-Flav-C2. Scheme depicts reaction to generate irradiated (Irr)-Mito-Flav-C2 following exposure of Mito-Flav-C2 to light (380-450 nm and 2450 lux of light power) for 24 h in the presence of oxygen. Red text indicates proposed source of new oxygen atoms in the product based on prior analysis of the reactivity of Flav-1.

binding of photoCORMs to serum proteins. The concentration of free photoCORMs available for cellular uptake was likely to be substantially lower.

Generation of photodegraded products. Flav-1, Mito-Flav-C2, and Mito-Flav-C8 were subjected to light exposure for 24 h using a Rayonet (Branford, CT) photoreactor equipped with eight RPR-4190A lamps. These lamps emitted light in a wavelength range of 380-450 nm with an excitation maximum at 419 nm. The light intensity power of the

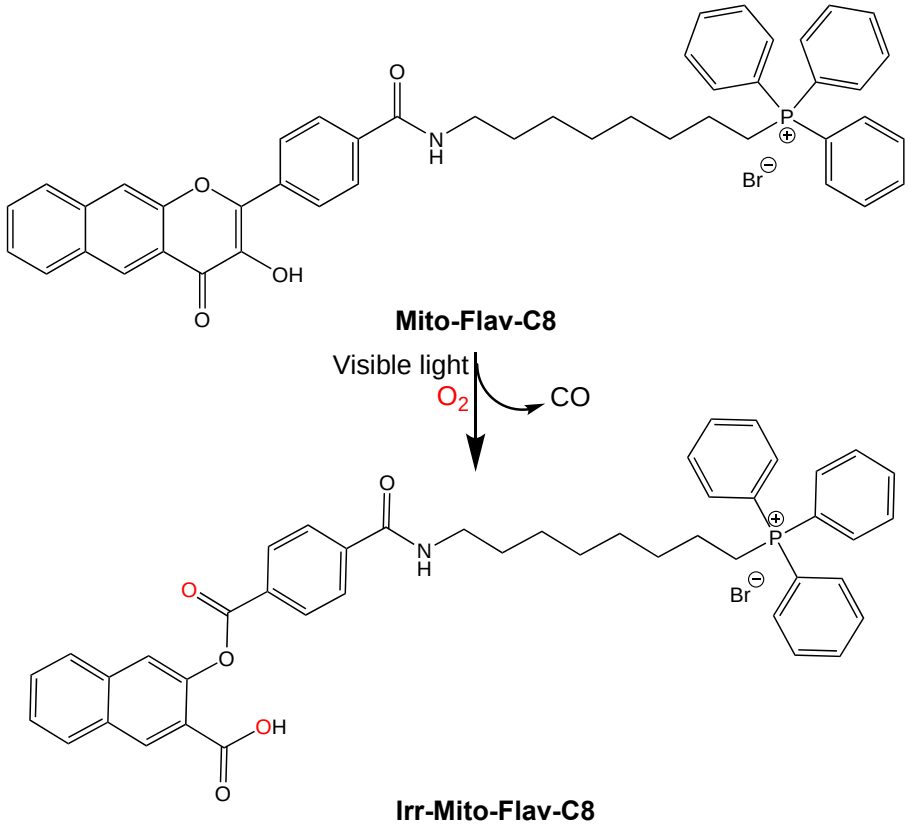

Figure 14. Photodegradation reaction of Mito-Flav-C8. Scheme depicts reaction to generate irradiated (Irr)-Mito-Flav-C8 following exposure of Mito-Flav-C8 to light (380-450 nm and 2450 lux of light power) for 24 h in the presence of oxygen. Red text indicates proposed source of new oxygen atoms in the product based on prior analysis of the reactivity of Flav-1.

photoreactor was measured using an Apogee Instruments (Logan, UT) MQ-500 full spectrum quantum meter and was determined to be 2450 lx (lumens per meter squared). The photodegraded products of Flav-1, Mito-Flav-C2, and Mito-Flav-C8 (indicated by irr- prefix) were used in experiments to compare the cytotoxicity of the parent compound and the light-induced product. Completion of the photochemical reaction was confirmed by ^{1}H NMR (Figures A9-A10). Schemes outlining the proposed reactions of Mito-Flav-

C2 and Mito-Flav-C8 to generate irradiated products following exposure to visible light are provided in Figures 13-14.

Cell culture. Human umbilical vein endothelial cells (HUVECs) were selected because they are a well-established primary cell line model suitable for *in vitro* oxidative stress studies. HUVECs are known to experience oxidative stress and altered mitochondrial respiration in disease states, such as vascular disease. CO is well known for its vasoprotective and vasodilatory capacity, in addition to reducing oxidative stress damage (Garcia-Gallego and Bernardes, 2014). HUVECs were obtained from ATCC (Manassas, VA, Cat. No. CRL-1730). Cells were cultured in F-12K medium (Gibco, Carlsbad, CA) supplemented with 0.03 mg/ml endothelial cell growth supplement (Sigma-Aldrich, St. Louis, MO), 10% (v/v) FBS, 0.1 mg/ml heparin (Sigma-Aldrich), and 100 U/ml streptomycin-penicillin solution (Gibco) in a humidified incubator at 37 ℃ with 5% CO_2. Complete media was replenished every three days, and cells were sub-cultured into T-75 flasks when they attained 90% confluence. At sub-culture, cells were detached by adding 3 ml of Trypsin-EDTA 1X solution (Caisson Laboratories) for 3-5 min, then neutralized with 8 ml of fresh media. HUVECs were counted using a Cell Countess instrument (Thermo Fisher Scientific, Boston, MA) according to the manufacturer's protocol. The minimum seeding density used to sub-culture into T-75 flasks was 4,000 cells/cm^2. HUVECs at passages one through eight were used in all experiments.

Human lung adenocarcinoma epithelial cells (A549) are a well-characterized cancer cell line used in many cytotoxicity experiments for their rapid and robust *in vitro*

growth. Also, this cell line has been used in prior studies with flavonol-based compounds, such as quercetin (e.g., Andreescu *et al.*, 2005; Zerin *et al.*, 2013). A549 cells were obtained from ATCC (Cat. No. CCL-185). Cells were cultured in phenol red-free DMEM-F12 media (Caisson Laboratories) supplemented with 10% FBS in a humidified incubator at 37 °C with 5% CO_2. Complete media was replenished every three days, and cells were sub-cultured into T-75 flasks when they attained 90% confluence. At sub-culture, cells were detached by adding 3.5 ml of Trypsin-EDTA 1X solution (Caisson Laboratories) for 5-10 min, then neutralized with 8 ml of fresh media. The minimum seeding density used to sub-culture into T-75 was 2,000 cells/cm^2. Cell counts were performed in the same manner as HUVECs.

Cytotoxicity assays. Cell viability was assessed using the 3-(4,5-dimethylthiazol-2-yl)-2,5-diphenyltetrazolium bromide (MTT) assay. The MTT assay is a well-established cytotoxicity assay used to detect the reduction of MTT to formazan by NADPH-dependent oxidoreductases, an indicator of cellular viability (Tolosa *et al.*, 2015). HUVEC or A549 cells were seeded in 96-well tissue culture plates at a density of 10,000 cells/well and in a volume of 190 µl/well and then allowed to attach for 24 h. Cells were then treated in triplicate with Mito-Flav-C2, Mito-Flav-C8, Flav-1, or their irradiated versions at concentrations ranging from 0.08 µM to 100 µM and incubated for 24 h. During and after the addition of light-sensitive chemicals, all plates were handled in a dark room and performed in triplicates. Mito-Flav-C2, Mito-Flav-C8, and their irradiated versions were solubilized in dimethylsulfoxide (DMSO) or ethanol and added to cells at a final concentration of 0.4% and 0.2% (v/v), respectively. Flav-1 and Irr-

Flav-1 were solubilized in DMSO and added to cells at a final concentration of 0.4% (v/v).

MTT (Sigma-Aldrich) was prepared fresh at 5 mg/ml in sterile phosphate-buffered solution (PBS), and then passed through a 0.22 µm polyethersulfone filter. Cells were then treated with 20 µl/well of MTT solution and placed in an incubator at 37 °C and 5% CO_2 for 4 h. Then, cell culture media was removed, and 200 µl/well of DMSO was added and mixed to solubilize the formazan pellets. Finally, the plates were placed in a Turner Biosystems Modulus™ Microplate reader (Promega Corp., Madison, WI) and absorbance was measured at 560 nm and 750 nm (background). Background-subtracted absorbance values were normalized to the vehicle control (0.4% DMSO).

Cytotoxicity data were analyzed using GraphPad Prism version 7 (La Jolla, California). The half-maximal inhibitory concentration (IC_{50}) was defined as the concentration at which the tested compound inhibited cell growth to 50% of the control. These concentrations were calculated using a four-parameter nonlinear regression with the bottom of the curve constrained to zero. For each chemical tested, a one-way ANOVA with Tukey post hoc test was used to compare cytotoxicity values to the lowest concentration tested to determine the lowest concentration of photoCORM that produced a detectable reduction in cell viability.

The Pierce Lactate Dehydrogenase (LDH) Assay Kit (Thermo Fisher Scientific) was used per the manufacturer's recommended protocol. The LDH assay is also a widely accepted and standard cell viability assay, which measures extracellular LDH released by cells with a compromised plasma membrane (Korzeniewski and Callewaert, 1983).

Briefly, HUVECs were optimized to a cell density of 8,000 cells/cm^2 to account for variability between cell lines in respect to LDH activity in the extracellular environment. The 96-well plates were seeded in a volume of 190 µl/well and allowed to attach for 24 h. Cells were then treated in triplicate with Mito-Flav-C2, Mito-Flav-C8 or Flav-1 and their irradiated versions at concentrations ranging from 0.08 µM to 100 µM with a final DMSO concentration of 0.4% (v/v) and then incubated for 24 h in the dark. The samples were placed in the microplate reader, and absorbance was measured at 450 nm and 750 nm. Background-subtracted absorbance values were normalized to the vehicle control (0.4% DMSO). Per the manufacturer's protocol, percent cytotoxicity was calculated by subtracting the LDH activity of the spontaneous LDH release control (vehicle-treated) from the LDH activity of chemical-treated sample, dividing by the total LDH activity [(maximum LDH release control activity) – (spontaneous LDH release control activity)], and multiplying by 100. Analysis of LDH cytotoxicity data was performed as described previously for MTT assays.

Confocal microscopy. HUVEC or A549 cells were sub-cultured at 100,000 cells/cm^2 and incubated for 24 h to allow for proper adherence. Cells were then treated with Mito-Flav-C2, Mito-Flav-C8, or Flav-1 and incubated for an additional 4 h. Afterward, cells were washed thrice with fresh media, the appropriate co-stains were added, and the cells were incubated for 15 min at 37 °C. Finally, the cells were washed thrice with fresh media and then imaged using a Zeiss LSM 710 confocal microscope (Thornwood, NY). The images were acquired using a 20x or 63x oil immersion objective with the following excitation lasers and emission ranges: Hoechst 33342 Stain (405

nm/410-492 nm); Mito-Flav-C2, Mito-Flav-C8 or Flav-1 (488 nm/495-581 nm); and MitoTracker Red CMXRos (561 nm/579-600 nm). Gain and laser intensity were adjusted to obtain the best signal-to-noise ratio. To enhance visualization, the reference dye channels (Hoechst 33342 and MitoTracker Red CMXRos) were adjusted by using the "best-fit" parameter available in the Zeiss Zen 2.3 Lite software (Thornwood, NY).

Preliminary confocal experiments with Mito-Flav-C8 solubilized in ethanol. Several initial confocal experiments were performed using Mito-Flav-C8 solubilized in ethanol at a final concentration of 0.2% (v/v) on cells grown in 4-well Millicell® E-Z Slides obtained from Millipore (Billerica, MA). However, the fluorescence signal was markedly lower compared to Mito-Flav-C8 solubilized in DMSO, and the stock solution of Mito-Flav-C8 prepared in 100% ethanol would not consistently remain dissolved (data not shown). Thus, all further microscopy experiments used CORMs solubilized in DMSO.

Qualitative assessment of emission intensity of photoCORMs in vitro. HUVEC and A549 cells were sub-cultured in 4-well Millicell® E-Z Slides and allowed to adhere for 24 h. Each chamber had a final volume of 850 µl of media. Cells were treated with 25-100 µM of Mito-Flav-C2, Mito-Flav-C8, or Flav-1 prepared in DMSO (≤0.4% (v/v) final concentration in media), and co-stained with 0.5% (v/v) Hoechst 33342 (ImmunoChemistry Technologies, LLC, Bloomington, MN). Both cell lines were incubated, washed, and imaged as outlined above.

Photodegradation of Mito-Flav-C2. A549 cells were sub-cultured in 35 mm glass bottom dishes obtained from MatTek (Ashland, MA) and allowed to adhere for 24 h for

live cell imaging. Cells were treated with 25 µM Mito-Flav-C2 in DMSO (0.1% (v/v) final concentration in media) and co-stained with 0.5% (v/v) Hoechst 33342. An initial image was obtained prior to laser light exposure. Images were then acquired every 5 min of continuous exposure to 405 and/or 488 nm lasers. A loss of fluorescence emission was indicative of CO release. A549 cells were incubated, washed, and imaged as outlined above.

Mitochondrial targeting of Mito-Flav-C2 and Mito-Flav-C8. HUVEC and A549 cells were sub-cultured in 4-well Millicell® E-Z Slides and allowed to adhere for 24 h. Each chamber had a final volume of 850 µl of media. Cells were treated with 100 µM Mito-Flav-C2, Mito-Flav-C8, or Flav-1 prepared in DMSO (0.4% (v/v) final concentration in media), and co-stained with 0.5% (v/v) Hoechst 33342 and 300 nM MitoTracker Red CMXRos (Thermo Fisher Scientific). Both cell lines were incubated, washed, and imaged as outlined above. In addition, a set of higher magnification images was acquired to enhance visualization of mitochondria morphology in A549 cells treated with 75 µM of Mito-Flav-C2 (0.3% (v/v) final concentration in media). Software image capture settings (Zeiss Zen 2.3 Lite) were adjusted to obtain higher magnification images, including increased pixel dwell time (greater photon capture), increased total pixels captured and increased zoom factor (set to 2x).

RESULTS

Cytotoxicity determined by the MTT assay. Two cytotoxicity assays were employed to compare the toxicity of the parent CORM structure, Flav-1, and the two TPP tail-modified structures, Mito-Flav-C2 and Mito-Flav-C8, in both HUVEC and A549 cells. First, as reported previously (Anderson, *et al.*, 2015), Flav-1 was observed to be moderately toxic to A549 cells, with an average IC_{50} value of 80.2±3.3 μM (Table 2; Figure 15A). The highest Flav-1 concentration of 100 μM reduced cell survival by 62% after 24 h, whereas concentrations lower than 10 μM did not alter cell viability. Irradiation of this CORM with visible light, which triggers release of CO, eliminated the apparent moderate toxicity of Flav-1, as treatment of A549 cells with Irr-Flav-1 for 24 h did not appreciably decrease the number of viable cells compared to vehicle control

Table 2. Calculated IC_{50} Values for Flav-1, Mito-Flav-C2 and Mito-Flav-C8 in A549 and HUVEC Cells as Determined by the MTT Assay.

	Flav-1		Mito-Flav-C2		Mito-Flav-C8	
	Parent	Irradiated	Parent	Irradiated	Parent	Irradiated
A549	80.2±3.3	ND	14.1±2.7	ND	8.48±4.0	69.1±11
HUVEC						
DMSO	L	ND	1.51±1.4	L	8.40±3.6	90.0±7.5
EtOH			L	L	31.9±14	108±14

IC_{50} values were calculated by non-linear regression analysis (four-parameter, variable slope) was performed (GraphPad Prism v. 7, La Jolla, CA) to generate the concentration-response curve for each chemical using each cell line. Values represent the mean ± SEM (n = 3 independent experiments, except n = 6 for Flav-1 in A549 cells). ND, no significant decrease in cell viability; L, less than 50% decrease in cell viability.

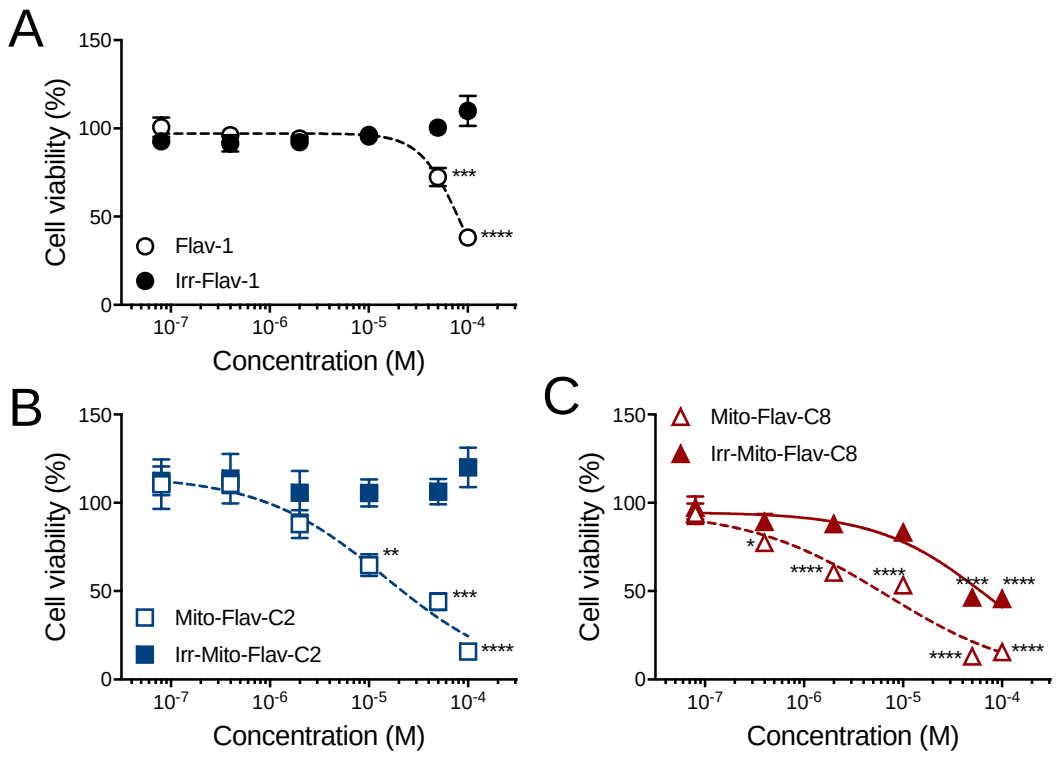

Figure 15. Toxicity of Flav-1, Mito-Flav-C2, Mito-Flav-C8, and their irradiated products in A549 cells measured by the MTT assay. Values shown are the mean ± SEM percent viability of cells with respect to the control (0.4% DMSO) for various concentrations of Flav-1 (A), Mito-Flav-C2 (B) and Mito-Flav-C8 (C). Cell viability data and non-linear regression analyses (four-parameter, variable slope) are shown for the native compounds (open symbols, dashed lines) and their photo-degraded products denoted with irr- prefix (closed symbols, solid lines). Error bars not visible are smaller than the symbol size. Panel A, $n = 6$ replicate experiments; panels B-C, $n = 3$ replicate experiments. *, $p<0.05$; **, $p<0.01$; ***, $p<0.001$; ****, $p<0.0001$ as determined by one-way ANOVA for each compound as compared to lowest concentration tested, 0.08 μM.

(Figure 15A). Because cell viability was greater than 50% at all test concentrations of Irr-Flav-1, an IC_{50} value was not determined.

Modification of the core Flav-1 structure by addition of the TPP tail moiety with either two (C2) or eight carbons (C8) altered the apparent toxicity of this CORM as determined by the MTT assay in A549 cells. Both Mito-Flav-C2 and -C8 were more

toxic than the core structure, with mean IC_{50} values of 14.1±2.7 and 8.48±4.0 μM, respectively, (Figure 15B-C; Table 2). At the highest concentration tested, cell viability was reduced by about 85% for both compounds. Unlike Flav-1 (Hillslope of -2.2), the slopes of the concentration-response curves for the TPP-modified structures were not as steep (Hillslope values of -0.68 and -0.78, respectively), such that low micromolar concentrations of Mito-Flav-C2 and -C8 also significantly reduced cell viability. Of note, irradiation of Mito-Flav-C2 completely ameliorated its apparent cytotoxicity, as no decrease in cell viability was evident (Figure 15B). However, irradiation of Mito-Flav-C8 was not as effective, as this compound retained moderate toxicity with an estimated IC_{50} value of 69.1±11 μM. Compared to its parent compound, Irr-Mito-Flav-C8 was substantially less toxic, as concentrations ≤ 10 μM did not significantly reduce cell viability (Figure 15C).

The base Flav-1 structure was less cytotoxic in HUVECs compared to the A549 cancer cell line, with a maximum decrease in cell viability of 35% at 100 μM and no apparent decrease at lower concentrations (Figure 16A). However, the irradiated compound was similarly not cytotoxic, with no apparent decrease in cell viability. As was observed in A549 cells, the TPP-modified structures were considerably more cytotoxic in HUVECs than the core structure, Flav-1 (Figure 16). However, the relative toxicity of the mitochondria-targeted CORMs differed depending on the solvent, EtOH or DMSO, used to deliver Mito-Flav-C2 and -C8 to cells. First, Mito-Flav-C2 delivered via DMSO significantly decreased cell viability by up to 77% with a mean IC_{50} value of 1.51±1.4 μM (Figure 16B). On the other hand, viability of HUVECs treated with Mito-

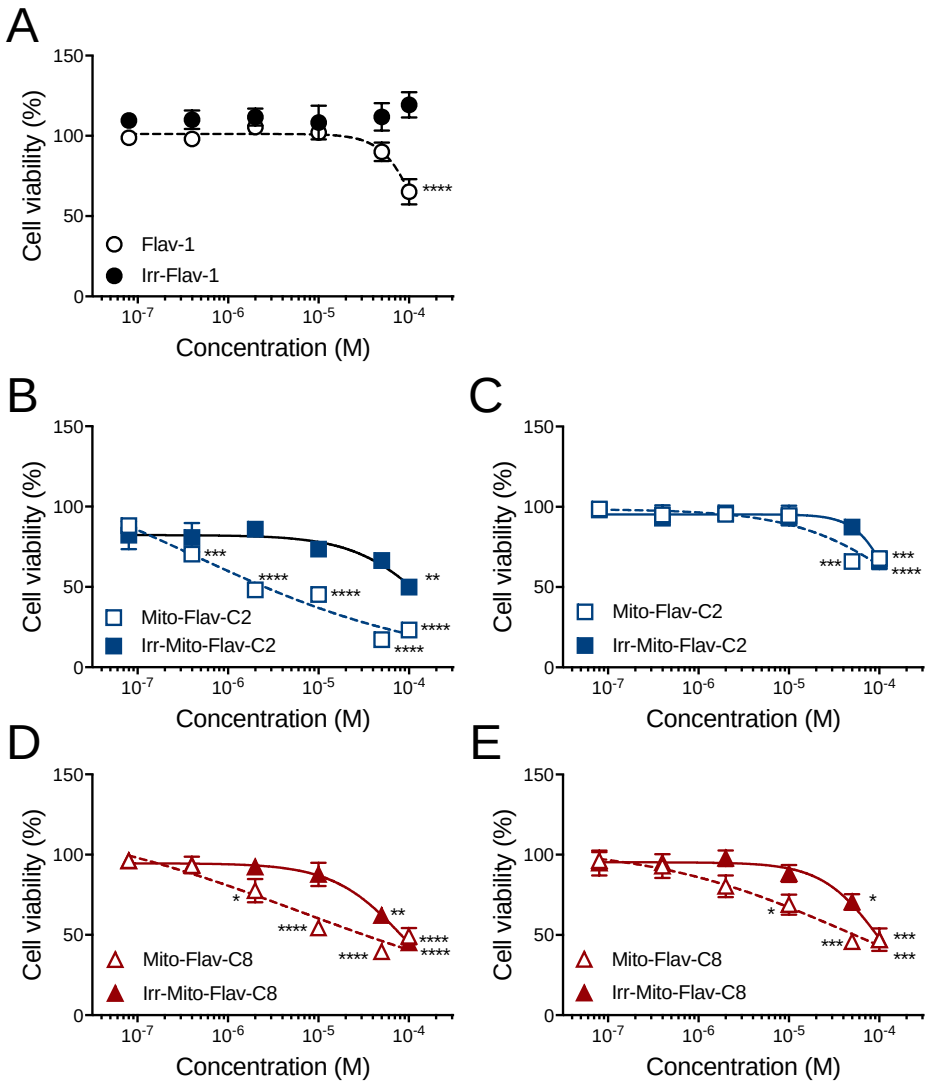

Figure 16. Toxicity of Flav-1, Mito-Flav-C2, Mito-Flav-C8, and their irradiated products in HUVECs measured by the MTT assay. Values shown are the mean ± SEM percent viability of cells with respect to the control (0.4% DMSO for panels A, B, and D; 0.2% EtOH for panels C and E) for various concentrations of Flav-1 (A), Mito-Flav-C2 (B-C) and Mito-Flav-C8 (D-E). Cell viability data and non-linear regression analyses (four-parameter, variable slope) are shown for the native compounds (open symbols, dashed lines) and their irradiated products denoted with irr- prefix (closed symbols, solid lines). Error bars not visible are smaller than the symbol size. Panel A, $n = 12$ replicate experiments; panels B-E, $n = 3$ replicate experiments. *, $p<0.05$; **, $p<0.01$; ***, $p<0.001$; ****, $p<0.0001$ as determined by one-way ANOVA for each compound as compared to lowest concentration tested, 0.08 μM.

Flav-C2 in EtOH was substantially greater, with a maximum decrease of only 34% observed at 100 μM (Figure 16C). As observed in A549 cells, irradiation of Mito-Flav-C2 markedly reduced the toxicity of the compound, with no apparent decrease in cell survival at concentrations ≤50 μM, irrespective of the solvent used (Figure 16B-C).

A different pattern was seen for Mito-Flav-C8, which decreased survival of HUVECs by 51% and 54% when delivered via DMSO or EtOH, respectively. In HUVECs, the average IC_{50} value of 8.40±3.6 μM for Mito-Flav-C8 in DMSO was very similar to that observed for A549 cells, whereas Mito-Flav-C8 delivered via EtOH resulted in a moderately higher IC_{50} value of 31.9±14 μM (Figure 16D-E). While irradiation of Mito-Flav-C8 markedly decreased the average IC_{50} (90.0±7.5 and 108±14 μM in DMSO and EtOH, respectively), the high concentration of 100 μM was similarly cytotoxic as the non-irradiated compound. However, Irr-Mito-Flav-C8 did not decrease cell viability at concentrations below 10 μM, as reflected by the apparent differences in the estimated Hillslopes for the regression curves (-0.28 or -0.34 for non-irradiated compared to -1.099 or 1.367 for irradiated Mito-Flav-C8 in solvents DMSO or EtOH, respectively).

Cytotoxicity determined by the LDH assay. A second cell viability assay was used to evaluate the impact of Flav-1, Mito-Flav-C2 and Mito-Flav-C8 and their irradiated products in HUVECs. As shown in Figure 17, results of this assay suggest that Mito-Flav-C2 and -C8 were substantially less toxic as compared to results for similar experiments using the MTT assay, with a maximal decrease in viability of only 24% and

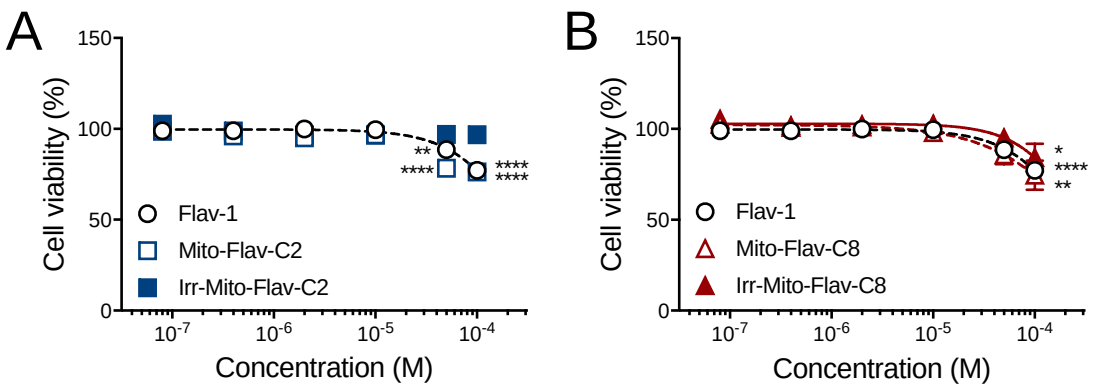

Figure 17. Toxicity of Flav-1, Mito-Flav-C2, Mito-Flav-C8, and their irradiated products in HUVECs measured by the LDH assay. Values shown are the mean ± SEM percent viability of cells with respect to the control (0.4% DMSO) for various concentrations of Flav-1, Mito-Flav-C2 (A) and Mito-Flav-C8 (B). Cell viability data and non-linear regression analyses (four-parameter, variable slope) are shown for the native compounds (open symbols, dashed lines) and their irradiated products denoted with irr- prefix (closed symbols, solid lines). (Irradiated Flav-1 not included in this assay). Error bars not visible are smaller than the symbol size. For both panels, $n = 5$ replicate experiments for Flav-1 and $n = 3$ replicate experiments for other compounds. *, $p<0.05$; **, $p<0.01$; ***, $p<0.001$; ****, $p<0.0001$ as determined by one-way ANOVA for each compound as compared to lowest concentration tested, 0.08 μM.

26%, respectively. However, none of the compounds tested reduced cell viability by more than 50%, and no IC_{50} values could be determined.

Visualization of CORM uptake and cellular localization by confocal microscopy. Using standard fluorescence microscopy, our group previously showed that incubation with high concentrations of Flav-1 led to the accumulation of this CORM in the cytoplasm of A549 cells (Anderson, *et al.*, 2015). In this study, we employed confocal microscopy to visualize uptake of Flav-1, Mito-Flav-C2, and Mito-Flav-C8 in both A549 and HUVEC cells. Initial experiments focused on identifying the appropriate conditions for loading these CORMs into the target cells and visualization by the confocal

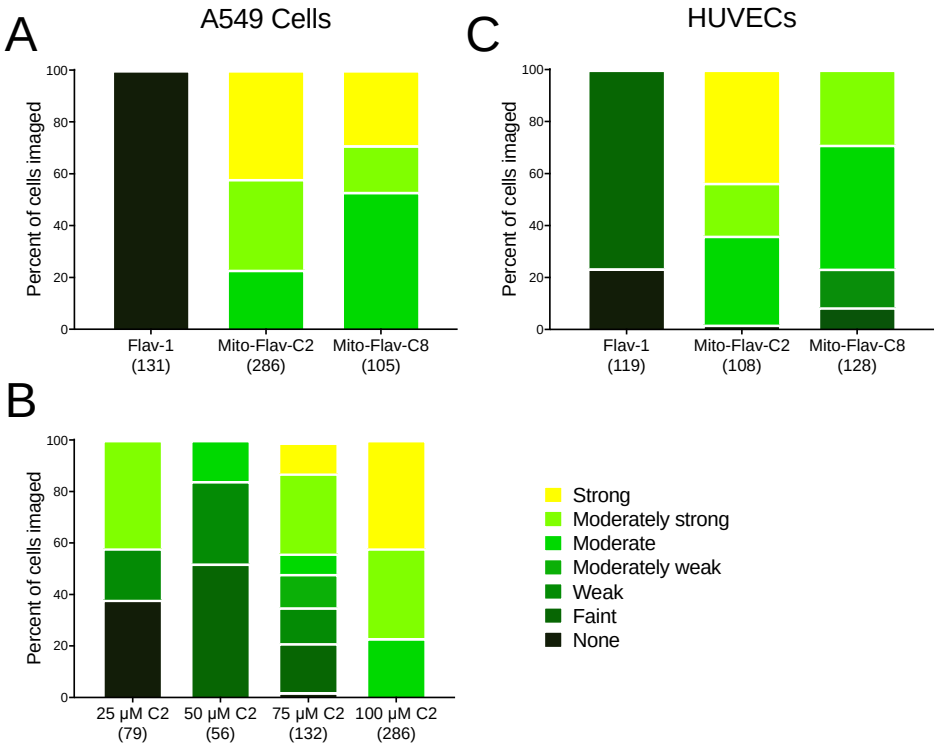

Figure 18. Qualitative assessment fluorescence emission intensity of photoCORMs in A549 cells and HUVECs. Signal intensity of Flav-1, Mito-Flav-C2, or Mito-Flav-C8 of A549 cells (A, B) or HUVECs (C). Cells in panels A and C were incubated for 4 h with 100 µM of each CORM, while cells in panel B were incubated for 4 h with 25 to 100 µM of Mito-Flav-C2. The strength of signal was assessed qualitatively by two individuals, and the numbers of cells imaged for each treatment is indicated in parentheses.

microscope, including varying the compound concentration and the time of incubation. Data presented in Figure 18 and summarized in Table A1 give an overall assessment of the entire data collection for confocal microscopy imaging of these CORMs. Fluorescence signal intensity was ranked using the following qualitative terms: strong, moderately strong, moderate, moderately weak, weak, faint, and no signals. The initial experiments assessed a 1 h or 4 h incubation period in complete culture media. Cells were also treated with 25 µM to 100 µM Mito-Flav-C2 to determine if a concentration

response could be visualized. An optimal fluorescence signal was obtained for cells treated with 75 µM or 100 µM, while a loading time of 4 h was determined to be most suitable for Mito-Flav-C2 and Mito-Flav-C8 for both cell lines. As indicated in Figure 18 and visualized in Figure 19E, no light emission for Flav-1 in A549 cells was

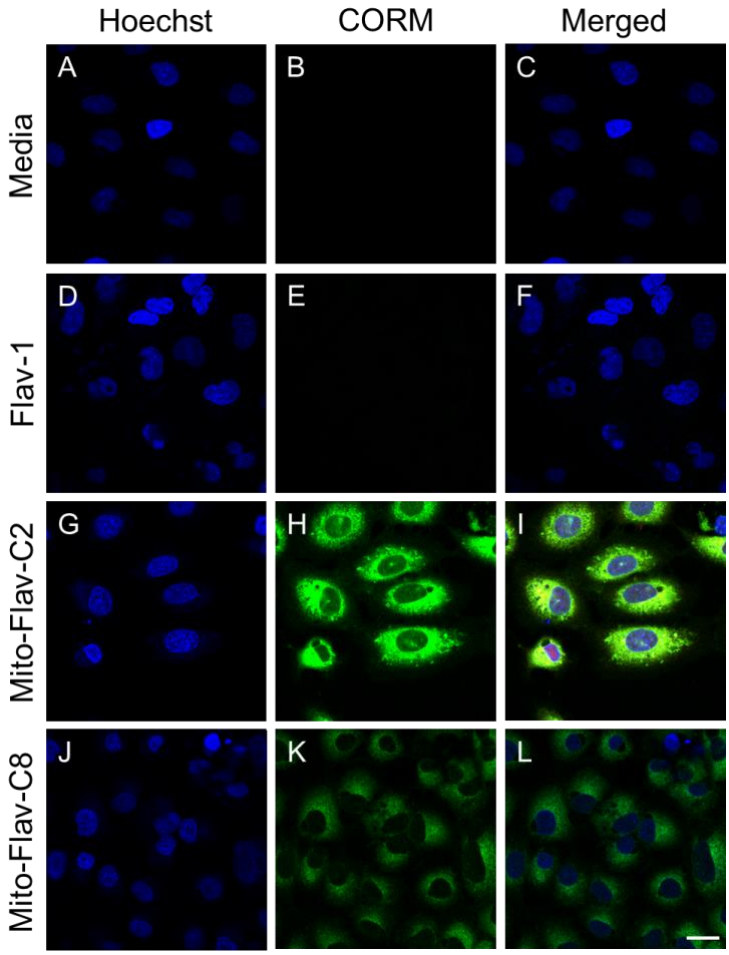

Figure 19. Confocal microscopy depicting cellular uptake of Flav-1, Mito-Flav-C2, and Mito-Flav-C8 in A549 cells. Cells were treated with vehicle media control (0.4% DMSO) (A-C), 100 µM Flav-1 (D-F), 100 µM Mito-Flav-C2 (G-I) or 100 µM Mito-Flav-C8 (J-L) for 4 h. Representative images shown depict the Hoechst 33342 nuclear stain (blue), the CORM (green) or a merge of the two fluorescence channels. Experiments were repeated at least three times, and a minimum of 21 cells were visualized for each experiment. Scale bar indicates 20 µm.

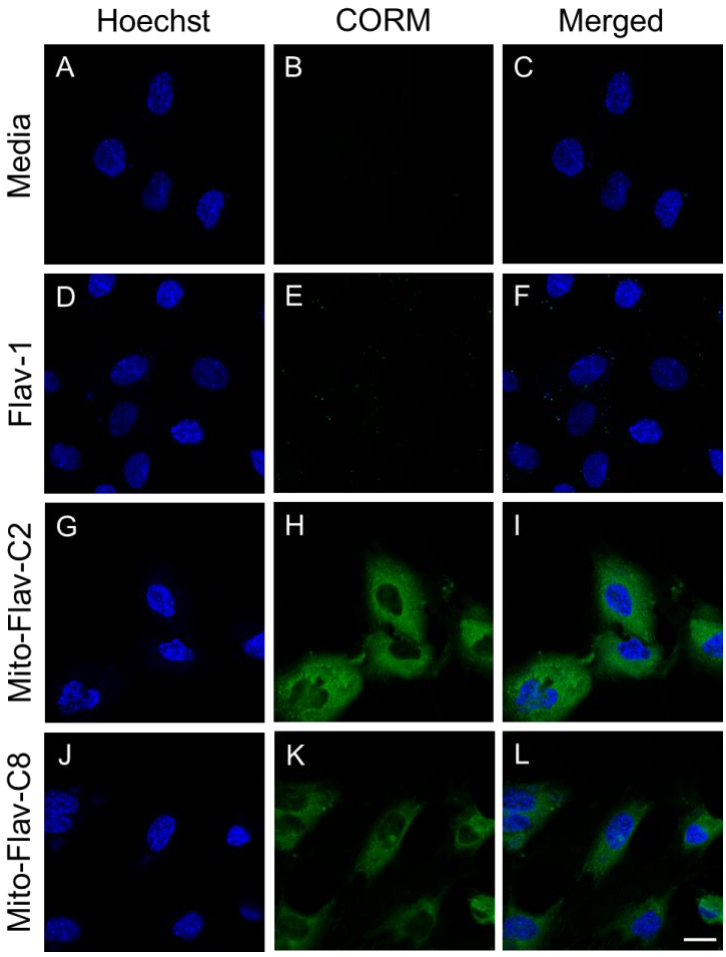

Figure 20. Confocal microscopy depicting cellular uptake of Flav-1, Mito-Flav-C2, and Mito-Flav-C8 in HUVECs. Cells were treated with vehicle media control (0.4% DMSO) (A-C), 100 µM Flav-1 (D-F), Mito-Flav-C2 (G-I) or Mito-Flav-C8 (J-L) for 4 h. Representative images shown depict the Hoechst 33342 nuclear stain (blue), the CORM (green) or a merge of the two fluorescence channels. Experiments were repeated at least three times, a minimum of 18 cells were visualized for each experiment. Scale bar indicates 20 µm.

detectable by confocal microscopy, and only a faint emission was evident in HUVECs (Figure 20E). However, strong emission intensity was clearly evident in both A549 cells and HUVECs treated with Mito-Flav-C2 (Figures 19H, 20H), and light emission intensity was positively correlated with the concentration of Mito-Flav-C2 in A549 cells (Figure

18B). Alternatively, the emission intensity for Mito-Flav-C8 was moderately diminished as compared to -C2, with only 47% of the A549 cells imaged having a strong or moderately strong signal for the longer tailed compound compared to 77% of cells for the short-tailed CORM (Figures 18A, 19K). In HUVECs, emission intensity for cells treated with 100 μM of the -C2 modified compound was qualitatively greater (43.5% of cells with strong intensity) compared to those treated with the -C8 modified CORM (0% of cells with strong intensity) (Figures 18C, 20K). Overall, these data suggest that, at the same loading concentration, the emission signal for Mito-Flav-C2 was more robust in

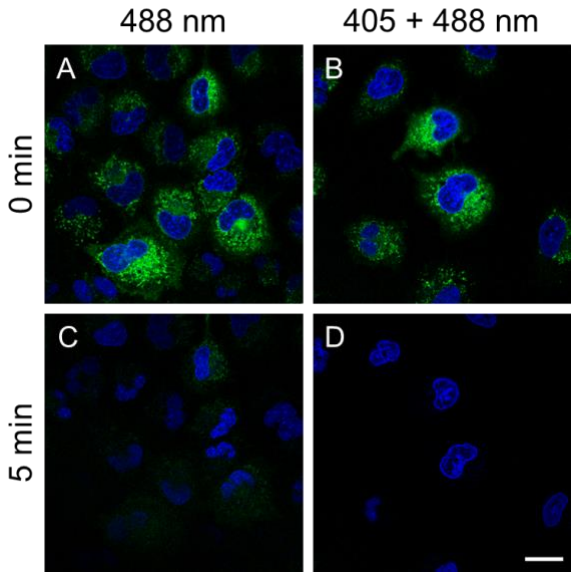

Figure 21. Light induced photodegradation of Mito-Flav-C2. A549 cells were treated with 25 μM Mito-Flav-C2 in 0.1% DMSO for 4 h, then counterstained with Hoechst 33342 prior to confocal microscopy. After obtaining initial images at wavelengths 410-492 nm for the nuclear stain (blue) and 495-611 nm for the CORM (green) (A-B), the cells were exposed to light at wavelength 488 nm (C) or 405 and 488 nm (D) for 5 min and then re-imaged. Images are representative of 79 total cells visualized over one experiment. Scale bar indicates 20 μm.

both cell lines compared to Mito-Flav-C8, and both TPP-modified CORMs had substantially greater detection than the core Flav-1 structure.

The next objective was to determine whether light exposure via the confocal microscope would trigger CO release and loss of fluorescence emission at the measured range (495-581 nm). Incubation of A549 cells with 25 µM Mito-Flav-C2 for 4 h led to a moderately strong fluorescence signal (Figure 21) as compared to the prior experiment using a 100 µM concentration (Figure 19). Following a 5 min exposure to light at wavelength of 488 nm, nearly all Mito-Flav-C2 signal had disappeared (Figure 21C). A complete loss of fluorescence signal was apparent when cells were exposed to light at both 405 and 488 nm wavelengths for 5 min (Figure 21D). These results suggest that light-induced CO release can be achieved in cell culture, in a similar manner as cell-free based assays.

To assess co-localization, our experiments incorporated MitoTracker Red CMXRos (MTR) as a fluorescent stain due to its known localization in the mitochondria, which are mainly found in proximity to the nucleus (Buravkov *et al.*, 2014). Mito-Flav-C2 and Mito-Flav-C8 readily localized near the mitochondria of A549 cells treated with 100 µM of either CORM when incubated for 4 h, indicated by the yellow-orange color in the merged image (Figure 22H, L). Note that the strong emission intensity for Mito-Flav-C2 consistently masked the signal from MTR, yielding only bright yellow-green in the merged image (Figure 22H). There was no apparent overlap in light emission for MTR at the wavelengths for detection of CORM, assuring us that the signal detected for CORM was genuine (Figure 22C).

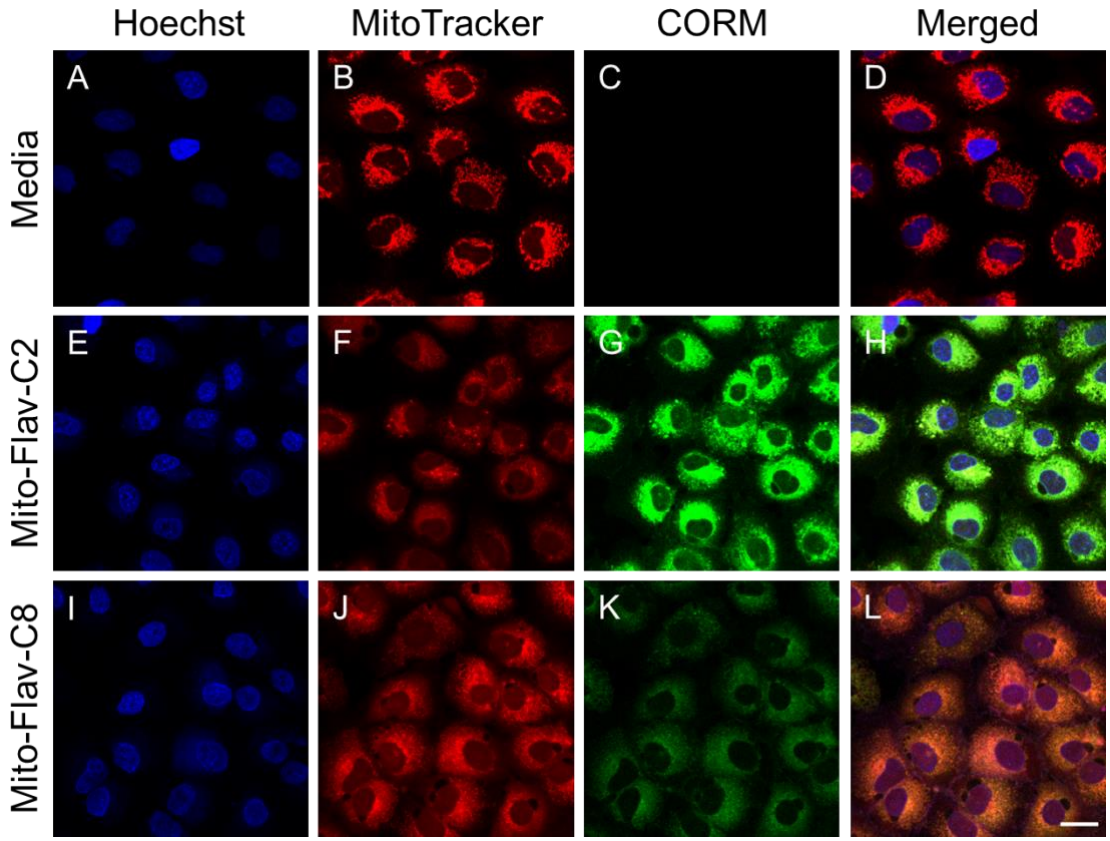

Figure 22. Co-localization of TPP-appended compounds with mitochondria in A549 cells. Cells were treated with vehicle control (0.4% DMSO) (A-D), 100 µM Mito-Flav-C2 (E-H) or Mito-Flav-C8 (I-L) for 4 h, then counterstained with Hoechst 33342 and MitoTracker Red CMXRos. Representative images shown depict the Hoechst nuclear stain (blue), the MitoTracker mitochondria stain (red) the CORM (green) or a merge of the three fluorescence channels. Experiments were repeated at least five times, and at least 21 cells were visualized for each experiment. Scale bar indicates 20 µm.

Importantly, the morphology of mitochondrial in cells treated with TPP-modified photoCORMs appeared to differ compared to cells incubated in plain media (Figure 22B, F, J). The structure of mitochondria in untreated cells was filamentous, whereas mitochondria in cells treated with Mito-Flav-C2 or -C8 tended to have a round shape. However, these pronounced effects on mitochondrial morphology were not as apparent at

25 µM Mito-Flav-C2 (Figure 21A and B). Additional experiments were performed at a higher magnification to observe in greater detail the mitochondrial morphology of A549 cells treated with Mito-Flav-C2 compared to media control (Figure 23). Notably, mitochondria of cells treated with 75 µM Mito-Flav-C2 appeared to swell and round up, losing their filamentous structure. Also, it was noted that the localization of this TPP-

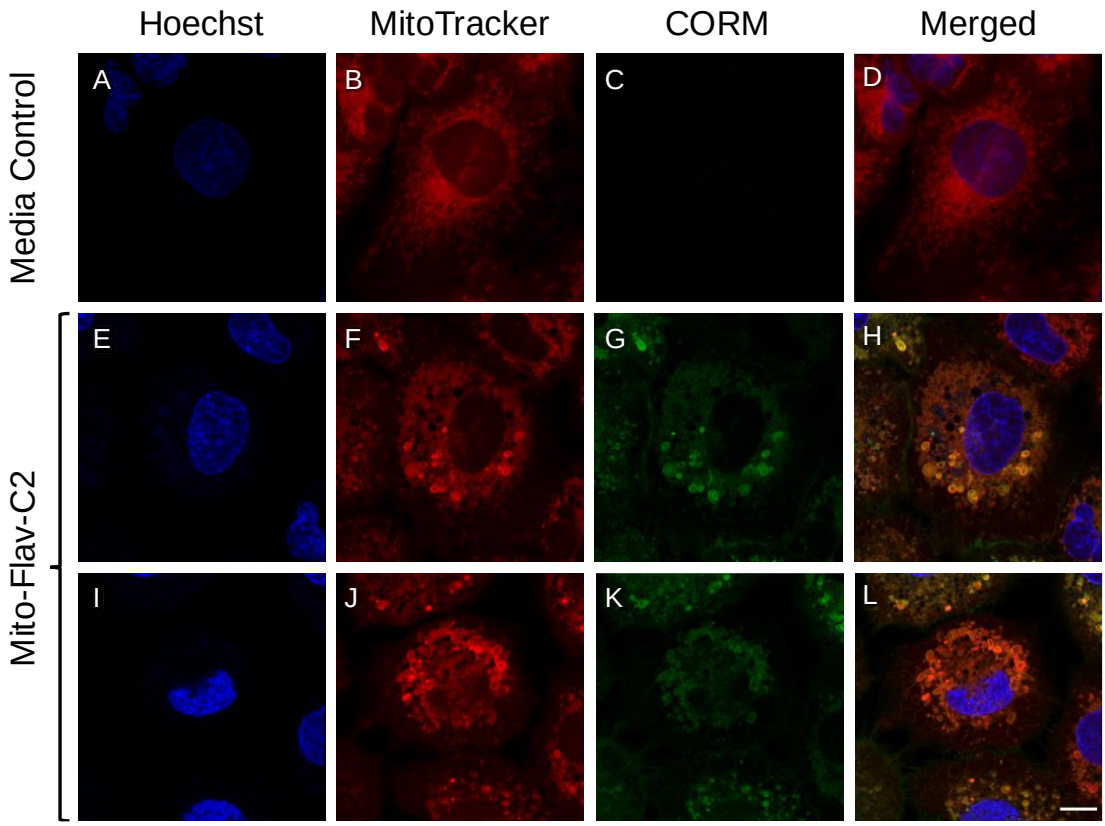

Figure 23. High magnification images showing Mito-Flav-C2's co-localization with and impact on mitochondria structure in A549 cells. Cells were treated with vehicle control (0.4% DMSO) (A-D) or 75 µM Mito-Flav-C2 (E-L) for 4 h, then counterstained with Hoechst 33342 and MitoTracker Red CMXRos. Images shown were obtained at 63× magnification and then subjected to a 2× digital zoom to better visualize subcellular structures. Image panels depict the Hoechst nuclear stain (blue), the MitoTracker mitochondria stain (red) the CORM (green) or a merge of the three fluorescence channels. Scale bar indicates 10 µm.

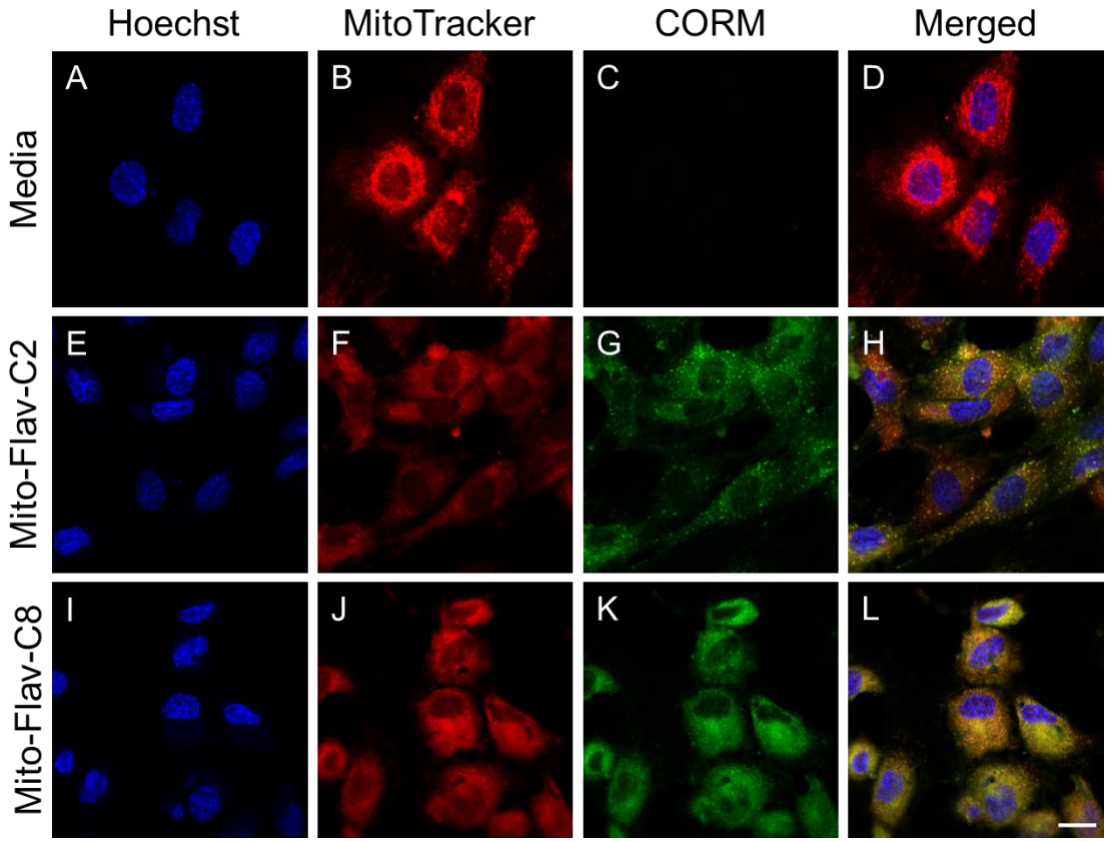

Figure 24. Co-localization of TPP-appended compounds with mitochondria in HUVEC cells. Cells were treated with vehicle control (0.4% DMSO) (A-D), 100 µM Mito-Flav-C2 (E-H) or Mito-Flav-C8 (I-L) for 4 h, then counterstained with Hoechst 33342 and MitoTracker Red CMXRos. Representative images shown depict the Hoechst nuclear stain (blue), the MitoTracker mitochondria stain (red) the CORM (green) or a merge of the three fluorescence channels. Experiments were repeated at least three times, and at least 18 cells were visualized for each experiment. Scale bar indicates 20 µm.

appended compound was closely aligned with MTR (Figure 23F, J), which was not as easily discerned at the higher test concentration.

Similar results for CORM co-localization with mitochondria were observed in HUVECs. Mito-Flav-C2 and Mito-Flav-C8 co-localized with the mitochondria as shown by the yellow-orange color in the merged image (Figure 24H, L). However, the emission

intensity in response to 100 μM Mito-Flav-C2 in HUVECs was not as pronounced as for A549 cells, and punctate localization throughout the cell was evident with partial overlap with the MTR signal (Figure 24G, H). Morphology of mitochondria in untreated cells remained filamentous, whereas mitochondria in CORM-treated cells were more spherical in shape (Figure 24B, F, J). No distinct differences in mitochondria shape were noted when comparing between the -C2 or -C8 CORM structures.

DISCUSSION

This study details the cytotoxicity and the localization of Flav-1 to the mitochondria of HUVEC and A549 cells after being modified with a TPP moiety. As such, these novel mitochondria-targeting photoCORMs represent the first CORMs with the capacity to target a specific organelle, which may have important applications in the study of the biological effects of CO. Furthermore, this work shows that the modified Mito-Flav-C2 and -C8 structures retained several desirable properties of the Flav-1 core structure, including light-triggered CO release, solubility in aqueous solution, and *in vitro* trackability by fluorescence light emission. The use of previous CORM structures has aided substantially in understanding the physiological importance of CO. However, these new photoCORMs that facilitate CO release in proximity of mitochondria may shed new light on the effects of this important gasotransmitter.

Several groups have recognized that certain features must be present in newer CORMs to fully understand the mechanistic aspects of CO and, thus, advance the study of the impact of CO on cellular physiology (Garcia-Gallego and Bernardes, 2014; Kautz, *et al.*, 2016; Mann, 2012; Motterlini and Foresti, 2017; Motterlini and Otterbein, 2010; Schatzschneider, 2015). Notably, these features include controlled and localized release of CO, a core structure amenable to chemical modification, and *in vitro* trackability, all of which are properties attributable to Flav-1. For example, the tunable nature of the Flav-1 core structure was recently demonstrated via the development of a "sense-of-logic" photoCORM, which is able to sense and react with free thiols, convert to Flav-1 and then release CO after exposure to visible light and oxygen (Soboleva *et al.*, 2017). Another

example of the structural tunability of Flav-1 was also shown by the development of zinc flavonolato complexes, which improved the photochemical properties of Flav-1 by coordination with a zinc(II) ion (Anderson *et al.*, 2016). The presence of the zinc ion red-shifted the absorption spectrum (required lower energy light for CO release) and increased the quantum yield (fewer photons absorbed per molecule of CO released). Also, addition of zinc provided for CO release when the compound was in the solid state and when solubilized, whereas the unmodified Flav-1 structure only released CO when in solution (Anderson, *et al.*, 2016). In the present study, by adding a TPP-tail moiety to Flav-1, we improved upon two key limitations of most current CORMs: spatial location and timing of release. In the field of gasotransmitters, only one other mitochondria-targeting molecule is currently available – a nitric oxide-releasing molecule that incorporates a TPP tail in its structure and has a carbon-dot motif to facilitate tracking by fluorescence emission (Xu *et al.*, 2015).

Results from the MTT cytotoxicity assays showed that Flav-1 was moderately toxic to A549 cells (similar to our prior observations (Anderson, *et al.*, 2015)), but the toxicity of this core structure was markedly decreased in HUVECs. Meanwhile, the irradiated version of Flav-1 did not impair viability of either cell line even at the highest tested concentration. The increased toxicity of Flav-1 in A549 cells could be explained by the aberrant metabolism characteristic of cancer cells, which typically display Warburg-like metabolism (high rates of glycolysis with cytosolic lactic acid fermentation) (Potter *et al.*, 2016). The addition of the TPP-tail to the core structure of Flav-1 moderately increased cytotoxicity of this CORM in both cell lines. Mito-Flav-C8

(in DMSO) had similar toxicity in both cell lines, while Mito-Flav-C2 (in DMSO) appeared more toxic in HUVECs than in A549 cells by an order of magnitude. Limited additional cytotoxicity assays were performed using EtOH as a vehicle for delivering the TPP-appended CORMs. However, we observed that solubility of Mito-Flav-C2 and -C8 was inconsistent for stock solutions prepared in ethanol. Therefore, the cytotoxicity data obtained for these CORMs delivered via ethanol to cells must be interpreted with caution. Also, an initial confocal imaging pilot experiment revealed a much-reduced fluorescence signal in cells treated with Mito-Flav-C8 prepared in ethanol compared to DMSO. Thus, DMSO was used as the vehicle for delivery of the photoCORMS for all further cell culture and confocal imaging experiments. As a polar aprotic solvent, DMSO was likely a more suitable carrier for these photoCORMs, which are somewhat hydrophobic and have limited capacity for forming hydrogen bonds. Moreover, DMSO is useful for delivering these hydrophobic compounds to cells by facilitating the transitions between the aqueous phase and the lipid membrane phase of the plasma membrane.

Other researchers employing the TPP motif have also assessed the impact of that structural modification on chemical cytotoxicity, with results broadly similar to those observed in this study. In their review, James and colleagues (2005) noted that MitoQ10, a TPP-tail modified co-enzyme Q10 molecule, was toxic to yeast at concentrations ≥1 µM, but that concentrations below 1 µM were not acutely toxic in mammalian cells. However, the effect of the length of the TPP-tail or the hydrophobicity of the TPP-appended compound on cells was unknown. Ross *et al.* (2008) compared the uptake of two hydrophobic TPP derivatives into mitochondria of intact cells, including MitoQ10

(termed MitoQ in their manuscript) and decylTPP (contains a 10-carbon tail), to the more hydrophilic TPP cation methyltriphenylphosphonium (TPMP) with a single carbon tail. They observed that uptake of MitoQ10 and DecylTPP occurred more rapidly (minutes as opposed to hours) and to a much greater extent than was observed for TPMP. In a later study, Reily *et al*. (2013) examined the effects of several mitochondrially-targeted antioxidants of varying TPP tail lengths on mitochondria bioenergetics in mouse mesangial cells to corresponding TPP structures that lacked the antioxidant group. They determined that the mitochondrial respiration rate was inversely correlated with alkyl chain length (greater inhibition at longer chain lengths) and with greater hydrophobicity. Similar results were observed by Trnka *et al*. (2015) using intact C2C12 myoblasts. In addition, these researchers noted a decrease in mitochondrial respiratory chain complexes when they treated rat skeletal muscle homogenates with 1 µM TPP with alkyl chains 10 or 12 carbons in length. Based on this observation, these authors expressed caution regarding the design of TPP-appended molecules due to the biologically active component of the TPP motif itself. Moreover, these moieties can adsorb to the matrix surface of the inner mitochondrial membrane, which may mediate their toxicity (Murphy and Smith, 2007). Thus, the addition of the TPP motif at high concentrations may cause cellular toxicity because of the effect of the TPP structure on mitochondrial respiration and integrity. Despite this apparent drawback, the TPP moiety may be useful for targeted delivery of signaling molecules, such as CO, to the mitochondria, as highlighted by other researchers (Graham, *et al.*, 2009; Logan and Murphy, 2017; Mattarei *et al.*, 2008; Murphy and Smith, 2007; Smith, *et al.*, 1999). Such may be the case for Mito-Flav-C2

or -C8, especially if a modulating effect can be achieved at substantially lower concentrations due to the proximity of CO release near its intracellular target organelles and/or molecules.

Although Mito-Flav-C2 and Mito-Flav-C8, as of now, are the first CORMs that can target mitochondria, other molecules have been synthesized with TPP-tails of varying lengths to deliver active compounds to mitochondria. Many of these molecules are already known for certain therapeutic properties. Notably, compounds modified to decrease mitochondrial production of reactive oxygen species include MitoSOD, MitoPeroxidase, MitoTEMPOL, MitoQ10, and MitoE2, which were designed to reduce O_2^-, H_2O_2, Fe^{2+}, and lipid peroxidation, respectively (Figure 8) (Murphy and Smith, 2007). For example, MitoE2 protected isolated rat mitochondria from oxidative damage more effectively than vitamin E alone (Smith, *et al.*, 1999). Similarly, Mattarei *et al.* (2008) synthesized a TPP-appended quercetin analogue, which had cytostatic and cytotoxic properties against murine colon cancer cells or fast-growing murine embryonic fibroblasts. Thus, TPP-tailed motifs are efficient modifications that allow selective accumulation to the mitochondria increasing their effectiveness against mitochondria induced oxidative damage.

Most CORM structures are metal carbonyls, and first-generation CORMs incorporated a manganese or ruthenium metal center (Figure 1). Later CORM structures incorporated other metals, such as iron, molybdenum, iridium, rhenium, tungsten, cobalt, or chromium, as well as boron as a metalloid (Kautz, *et al.*, 2016). Although many of these metals are present in the body as trace elements, the toxicity of the metal center

post-CO release has not been clearly evaluated for all compounds. Indeed, in some cases, the toxicity of the CO release reaction product(s) has not been assessed at all. For example, CORM-3, a widely-used CORM, has low apparent cytotoxicity with no observed significant effects on viability of porcine aortic endothelial cells or primate peripheral blood mononuclear cells at concentrations less than 500 μM as determined by the MTS assay (Vadori *et al.*, 2009). Despite the low toxicity of CORM-3 in these cell lines, therapeutic use may be difficult due to its complex solvent-dependent chemistry. At a physiological pH, CORM-3 forms several isomers and adducts that may prove difficult to track and may also have variable CO release kinetics (Schatzschneider, 2015). A study performed by Nobre *et al*. (2016) characterized several metal containing CORMs as generally non-toxic against murine macrophages (RAW 264.7), porcine kidney epithelial (LLC-PK1), and human hepatoma (HepG2) cells. Nobre and colleagues noted that concentrations greater than 50 μM of these metal-containing CORMs were required to induce significant cell death, while in some cases, no cell death was observed even at 500 μM, as determined by the MTT assay. Also using the MTT assay, Gong *et al*. (2016) showed that cobalt-based CORMs had IC_{50} values ranging from 36.2 to 125 μM in HeLa (cervical cancer) cells and 39.3 to 139 μM in HepG2 cells. The toxicity of iron-containing ET-CORMs was assessed by Romanski *et al*. (2013) in HUVEC and proximal tubular epithelial cells (PTEC). They observed that only two of the tested compounds were toxic at 100 μM, while most were only toxic at 1000 μM, also measured by the MTT assay. On the other hand, only two other organic photoCORMs have been reported: a diketone derivative, which requires micelle encapsulation for light-induced

release (Peng, *et al.*, 2013), and a xanthene-9-carboxylic acid compound that releases CO when irradiated with 500 nm light (Antony, *et al.*, 2013) (Figure 4). The diketone derivative was shown to be non-toxic up to the highest tested concentration of 40 μM in KG1 (leukemia) cells. However, the toxicity of the xanthene-9-carboxylic acid compound was not determined. Considering these available reports, the apparent cytotoxicity of Flav-1 in HUVECs is moderate as compared to other CORM structures. Alternatively, the higher toxicity reported for Mito-Flav-C2 and -C8 remains consistent with that of other TPP-appended compounds. Though this motif increases the apparent toxicity of the CORM structure, the capacity for mitochondrial targeting imparts an advantage that may overcome the limitation. It is conceivable that the tail may allow for accumulation of the CORM proximal to the mitochondria, so that one could achieve physiologically-relevant concentrations of CO near the metabolic systems with which it may interact at CORM concentrations that are not toxic to the overall cells. Thus, one may be able to achieve therapeutic effects of these biologically-based photoCORMs at concentrations well below those that cause adverse effects in cells. That said, to retain the utility of these CORMs for imaging at lower concentrations, the light emission intensity yield per molecule would need to be improved.

In this study, cytotoxicity of all three photoCORMs was estimated to be much lower using the LDH assay as compared to the MTT assay in HUVECs. A plausible explanation for this outcome is that the MTT assay measures mitochondrial respiration rate via conversion of tetrazolium salts into formazan dyes, while the LDH assay detects the release of LDH into the extracellular environment, which is indicative of membrane

damage. Thus, the MTT assay is a good indicator of dysfunctional mitochondrial bioenergetics, which typically leads to apoptosis, while the LDH assay is useful for assessing later stages of cell death, such as necrosis. Given the apparent difference in estimated cytotoxicity of these photoCORMs, it is possible that they triggered apoptosis in HUVECs during the 24 h period of incubation. Also, as discussed previously, the structure of the TPP-appended compounds may alter mitochondrial respiration. If the photoCORM induced a mild de-coupling of the electron transport chain leading to a reduced cellular respiration rate, then cell viability likely would be underestimated using the MTT assay. However, the impact of either Mito-Flav-C2 or Mito-Flav-C8 (prior to or after CO release) on mitochondrial respiration has yet to be determined.

Confocal microscopy confirmed uptake and co-localization of Mito-Flav-C2 and Mito-Flav-C8 to the mitochondria of HUVEC and A549 cells. Fluorescence intensity was stronger in Mito-Flav-C2 treated cells when compared to those incubated with Mito-Flav-C8, which may be indicative of greater cellular uptake by Mito-Flav-C2. Also, uptake of both compounds appeared greater in A549 cells. We noted that short-term incubation of cells with 100 μM Mito-Flav-C8 had a negative impact on cell morphology, despite the apparent increase in fluorescence intensity observed by confocal microscopy. In contrast, a short-term, 4 h incubation with Mito-Flav-C2 yielded a robust fluorescence signal without apparent cellular damage, and, thus, -C2 was the focus of the remaining imaging experiments. Also, the decreased accumulation of Mito-Flav-C8 in mitochondria as compared to Mito-Flav-C2 may be explained by the longer alkyl chain length, which decreases the mitochondrial membrane potential (Trnka, *et al.*, 2015). An

increase in membrane permeability of the mitochondria would lead to faster depolarization, which would affect the targeting capabilities of TPP-motifs by disrupting the electrical potential. Accumulation of TPP-appended compounds near mitochondria has been shown to be hindered by treatment with carbonyl-cyanide-p-trifluoromethoxyphenylhydrazone (FCCP), which is an ionophore that disrupts the electron transport chain (Ross, *et al.*, 2008). Furthermore, Mattarei *et al*. (2008), showed that treatment with 2 µM FCCP caused diffusion of TPP-appended quercetin analogues into the cytosol of HCT116 (colorectal carcinoma) cells. In addition to uptake and co-localization, treatment with Mito-Flav-C2 and -C8 caused substantial changes to mitochondrial morphology. High resolution confocal images of A549 cells treated with 75 µM Mito-Flav-C2 depicted enlarged, rounded mitochondria, indicative of high cellular stress. In contrast, mitochondria of untreated cells were tubular or filamentous in shape, indicative of metabolically active, normal-functioning mitochondria (Willems *et al.*, 2015). As explained previously, depolarization of the mitochondrial membrane (as with FCCP treatment) impairs the accumulation of TPP-appended compounds at the mitochondria. Increasing concentrations of these photoCORMs to facilitate visualization via fluorescence microscopy introduced a secondary problem of altered mitochondria morphology. Conversely, reducing the concentration of Mito-Flav-C2 and -C8 in cells may allow for greater accumulation at the mitochondria without triggering depolarization. However, low concentrations of these compounds might not be detectable by confocal microscopy due to exposure to laser light when acquiring an image or by low fluorescence intensity. Therefore, a balance between detection and

accumulation must be met. In practice, researchers using Mito-Flav-C2 or -C8 may load cells at high concentrations to optimize loading time and confirm cellular uptake, and then employ lower concentrations in cellular studies aimed to elucidate the biological effects of CO, such as studies of mitochondrial bioenergetics.

Interestingly, photo-degradation of Mito-Flav-C2 could be performed using 405 or 488 nm lasers, which modulated the time required to completely photodegrade the CORM. Also, photodegradation occurred when utilizing a bright-field source, which excited at a broad spectrum of visible light (data not shown). CO release from Mito-Flav-C2 was achieved very rapidly when exposed to both 405 and 488 nm lasers, was moderately slower when exposed to only 488 nm light, and was slowest when exposed to a bright-field source. Thus, CO release can be triggered without the use of near UV-light, unlike most photoCORMs (Wright and Wright, 2016). An ideal photoCORM will release CO when exposed to wavelengths above 600 nm (red and infrared regions) to maximize tissue penetration and avoid the damaging effects of high energy light.

Motterlini and Foresti (2017) noted the importance of CO release in the proximity of physiological targets. In their recent review, they observed that location of CO release (intra- or extracellularly) dictates the concentration required to produce physiological effects. Inhaled CO is the least effective method for CO delivery because exposure concentrations must be sufficiently high to overcome binding to circulating hemoglobin and myoglobin in order to reach peripheral tissues. Interestingly, CO released via CORMs is detectable by a CO sensor, namely COP-1, but a detectable concentration of CO is not triggered when heme oxygenase is induced by heme to produce endogenous

CO (unpublished observation reported by Motterlini and Foresti, 2017). However, the detection limit of COP-1 is about 1 μM, which may explain the inability of the probe to detect endogenously generated CO (Michel *et al.*, 2012). Recently, Liu *et al*. (2017) developed a near-infrared fluorescent probe (1-Ac) capable of detecting endogenously-produced CO. Their experiments showed that Raw 264.7 cells and zebrafish embryos cultured under hypoxic conditions produced a significantly higher fluorescent signal compared to normoxic culture conditions. In addition, the group further demonstrated the utility of their CO sensor by using 1-Ac to detect endogenous production of CO stimulated by induction of HO-1 with lipopolysaccharide and hemin in Balb/c mice (2017). In the future, this new molecular tool for sensing CO release *in vitro* and *in vivo* could be coupled with our new mitochondria-targeting photoCORMs for detailed molecular investigations on CO impacts on mitochondrial bioenergetics, reactive oxygen species generation, and subsequent cell signaling responses in the context of various disease states, such as cardiovascular disease or cancer.

In conclusion, this study, in collaboration with Berreau and colleagues, characterized and functionalized the first mitochondria-targeting CORM by adding a TPP motif to Flav-1. Furthermore, modification of Flav-1 with TPP motifs did not alter its desirable characteristics of visible light-induced CO release in the presence of oxygen, fluorescence emission, solubility at non-toxic concentrations of DMSO, and a clean reaction with no unknown by-products. Cytotoxicity of Mito-Flav-C2 and -C8, as determined by the MTT assay, in HUVEC and A549 cells was significantly increased by addition of the TPP tail compared to the base Flav-1 structure. However, this toxicity did

not differ substantially from other existing TPP-appended molecules, and this increase in toxicity may be due to an increase in uptake efficiency. Thus, increased cellular uptake could allow cells to be treated with lower concentrations of Mito-Flav-C2 or -C8 to achieve biological effects. Notably, confocal microscopy data showed that addition of the TPP tail to the Flav-1 core structure facilitated greater uptake and localization to the mitochondria of HUVEC and A549 cells, as expected. Interestingly, our data also demonstrated that Mito-Flav-C2 was subject to photodegradation using varying wavelengths of light and also a bright-field source, which may be used to trigger the release of CO.

As research with these photoCORMs continues, new areas of focus are clear. First, the most important next step is to assess the impact of Mito-Flav-C2 and -C8 and light-triggered CO release from these compounds on mitochondrial bioenergetics. Additionally, future work may include the use of 1-Ac or other CO reporters to assess the release of CO within cells because low concentrations of Mito-Flav-C2 and -C8 would not be detectable by their own fluorescence. Future cellular bioassays should also provide for comparisons between mitochondria-targeted photoCORMs and other CORMs that operate via ligand exchange or enzymatic trigger with respect to CO delivery and changes in cell physiology (e.g., production of reactive oxygen species and activation of oxidative stress response pathways). Lastly, this study exemplifies the successful structural modification of the core structure of a CORM to achieve additional utility as a molecular tool. Further modifications to the core structure may impart other desirable characteristics, such as addition of motifs for other organelle targeting, or other structural

modifications that improve the intensity of fluorescence emission, allow for CO release at lower energy wavelengths or that increase the yield of CO release per molecule of CORM.

REFERENCES

Al-Owais, M. M., Dallas, M. L., Boyle, J. P., Scragg, J. L., and Peers, C. (2015). Heme oxygenase-1 influences apoptosis via CO-mediated inhibition of K+ channels. *Adv. Exp. Med. Biol.* **860**, 343-351.

Almeida, A. S., Figueiredo-Pereira, C., and Vieira, H. L. (2015). Carbon monoxide and mitochondria-modulation of cell metabolism, redox response and cell death. *Front. Physiol.* **6**, 33.

Almeida, A. S., Queiroga, C. S., Sousa, M. F., Alves, P. M., and Vieira, H. L. (2012). Carbon monoxide modulates apoptosis by reinforcing oxidative metabolism in astrocytes: role of Bcl-2. *J. Biol. Chem.* **287**, 10761-10770.

Anderson, S. N., Larson, M. T., and Berreau, L. M. (2016). Solution or solid - it doesn't matter: visible light-induced CO release reactivity of zinc flavonolato complexes. *Dalton Trans.* **45**, 14570-14580.

Anderson, S. N., Richards, J. M., Esquer, H. J., Benninghoff, A. D., Arif, A. M., and Berreau, L. M. (2015). A structurally-tunable 3-hydroxyflavone motif for visible light-induced carbon monoxide-releasing molecules (CORMs). *ChemistryOpen* **4**, 590-594.

Andreescu, S., Sadik, O. A., and McGee, D. W. (2005). Effect of natural and synthetic estrogens on a549 lung cancer cells: correlation of chemical structures with cytotoxic effects. *Chem. Res. Toxicol.* **18**, 466-474.

Antony, L. A., Slanina, T., Sebej, P., Solomek, T., and Klan, P. (2013). Fluorescein analogue xanthene-9-carboxylic acid: a transition-metal-free CO releasing molecule activated by green light. *Org. Lett.* **15**, 4552-4555.

Brouard, S., Otterbein, L. E., Anrather, J., Tobiasch, E., Bach, F. H., Choi, A. M., and Soares, M. P. (2000). Carbon monoxide generated by heme oxygenase 1 suppresses endothelial cell apoptosis. *J. Exp. Med.* **192**, 1015-1026.

Buravkov, S. V., Pogodina, M. V., and Buravkova, L. B. (2014). Comparison of mitochondrial fluorescent dyes in stromal cells. *Bull. Exp. Biol. Med.* **157**, 654-658.

Chahar, M. K., Sharma, N., Dobhal, M. P., and Joshi, Y. C. (2011). Flavonoids: a versatile source of anticancer drugs. *Pharmacognosy Rev.* **5**, 1-12.

Chakraborty, I., Carrington, S. J., and Mascharak, P. K. (2014a). Design strategies to improve the sensitivity of photoactive metal carbonyl complexes (photoCORMs) to visible light and their potential as CO-donors to biological targets. *Acc. Chem. Res.* **47**, 2603-2611.

Chakraborty, I., Carrington, S. J., and Mascharak, P. K. (2014b). Photodelivery of CO by designed PhotoCORMs: correlation between absorption in the visible region and metal-CO bond labilization in carbonyl complexes. *ChemMedChem* **9**, 1266-1274.

Chapman, J. T., Otterbein, L. E., Elias, J. A., and Choi, A. M. (2001). Carbon monoxide attenuates aeroallergen-induced inflammation in mice. *Am. J. Physiol. Lung Cell Mol. Physiol.* **281**, L209-L216.

Crook, S. H., Mann, B. E., Meijer, A. J., Adams, H., Sawle, P., Scapens, D., and Motterlini, R. (2011). [Mn(CO)4{S2CNMe(CH2CO2H)}], a new water-soluble CO-releasing molecule. *Dalton Trans.* **40**, 4230-4235.

Garcia-Gallego, S., and Bernardes, G. J. (2014). Carbon-monoxide-releasing molecules for the delivery of therapeutic CO in vivo. *Angew. Chem. Int. Ed. Engl.* **53**, 9712-9721.

Gong, Y., Zhang, T., Li, M., Xi, N., Zheng, Y., Zhao, Q., Chen, Y., and Liu, B. (2016). Toxicity, bio-distribution and metabolism of CO-releasing molecules based on cobalt. *Free Radic. Biol. Med.* **97**, 362-374.

Graham, D., Huynh, N. N., Hamilton, C. A., Beattie, E., Smith, R. A., Cocheme, H. M., Murphy, M. P., and Dominiczak, A. F. (2009). Mitochondria-targeted antioxidant MitoQ10 improves endothelial function and attenuates cardiac hypertrophy. *Hypertension* **54**, 322-328.

James, A. M., Cocheme, H. M., Smith, R. A., and Murphy, M. P. (2005). Interactions of mitochondria-targeted and untargeted ubiquinones with the mitochondrial respiratory chain and reactive oxygen species. Implications for the use of exogenous ubiquinones as therapies and experimental tools. *J. Biol. Chem.* **280**, 21295-21312.

Ji, X., Ji, K., Chittavong, V., Yu, B., Pan, Z., and Wang, B. (2017). An esterase-activated click and release approach to metal-free CO-prodrugs. *Chem. Commun. (Camb.)* **53**, 8296-8299.

Ji, X., Zhou, C., Ji, K., Aghoghovbia, R. E., Pan, Z., Chittavong, V., Ke, B., and Wang, B. (2016). Click and release: a chemical strategy toward developing gasotransmitter prodrugs by using an intramolecular diels-alder reaction. *Angew. Chem. Int. Ed. Engl.* **55**, 15846-15851.

Jobsis, P. D., Rothstein, E. C., and Balaban, R. S. (2007). Limited utility of acetoxymethyl (AM)-based intracellular delivery systems, in vivo: interference by extracellular esterases. *J. Microsc.* **226**, 74-81.

Johnson, T. R., Mann, B. E., Teasdale, I. P., Adams, H., Foresti, R., Green, C. J., and Motterlini, R. (2007). Metal carbonyls as pharmaceuticals? [Ru(CO)(3)Cl(glycinate)], a CO-releasing molecule with an extensive aqueous solution chemistry. *Dalton Trans.* **0**, 1500-1508.

Kautz, A. C., Kunz, P. C., and Janiak, C. (2016). CO-releasing molecule (CORM) conjugate systems. *Dalton Trans.* **45**, 18045-18063.

Kim, H. J., Joe, Y., Yu, J. K., Chen, Y., Jeong, S. O., Mani, N., Cho, G. J., Pae, H. O., Ryter, S. W., and Chung, H. T. (2015). Carbon monoxide protects against hepatic ischemia/reperfusion injury by modulating the miR-34a/SIRT1 pathway. *Biochim. Biophys. Acta* **1852**, 1550-1559.

Korzeniewski, C., and Callewaert, D. M. (1983). An enzyme-release assay for natural cytotoxicity. *J. Immunol. Methods* **64**, 313-320.

Lancel, S., Hassoun, S. M., Favory, R., Decoster, B., Motterlini, R., and Neviere, R. (2009). Carbon monoxide rescues mice from lethal sepsis by supporting

mitochondrial energetic metabolism and activating mitochondrial biogenesis. *J. Pharmacol. Exp. Ther*. **329**, 641-648.

Liu, K., Kong, X., Ma, Y., and Lin, W. (2017). Rational Design of a Robust Fluorescent Probe for the Detection of Endogenous Carbon Monoxide in Living Zebrafish Embryos and Mouse Tissue. *Angew. Chem. Int. Ed. Engl.* **56**, 13489-13492.

Logan, A., and Murphy, M. P. (2017). Using chemical biology to assess and modulate mitochondria: progress and challenges. *Interface Focus* **7**, 20160151.

Mann, B. E. (2012). CO-releasing molecules: a personal view. *Organometallics* **31**, 5728-5735.

Marques, A. R., Kromer, L., Gallo, D. J., Penacho, N., Rodrigues, S. S., Seixas, J. D., Bernardes, G. J. L., Reis, P. M., Otterbein, S. L., Ruggieri, R. A., *et al.* (2012). Generation of carbon monoxide releasing molecules (CO-RMs) as drug candidates for the treatment of acute liver injury: targeting of CO-RMs to the liver. *Organometallics* **31**, 5810-5822.

Mattarei, A., Biasutto, L., Marotta, E., De Marchi, U., Sassi, N., Garbisa, S., Zoratti, M., and Paradisi, C. (2008). A mitochondriotropic derivative of quercetin: a strategy to increase the effectiveness of polyphenols. *ChemBioChem* **9**, 2633-2642.

Michel, B. W., Lippert, A. R., and Chang, C. J. (2012). A reaction-based fluorescent probe for selective imaging of carbon monoxide in living cells using a palladium-mediated carbonylation. *J. Am. Chem. Soc.* **134**, 15668-15671.

Motterlini, R. (2007). Carbon monoxide-releasing molecules (CO-RMs): vasodilatory, anti-ischaemic and anti-inflammatory activities. *Biochem. Soc. Trans.* **35**, 1142-1146.

Motterlini, R., and Foresti, R. (2017). Biological signaling by carbon monoxide and carbon monoxide-releasing molecules. *Am. J. Physiol. Cell Physiol.* **312**, C302-C313.

Motterlini, R., and Otterbein, L. E. (2010). The therapeutic potential of carbon monoxide. *Nat. Rev. Drug Discov.* **9**, 728-743.

Mu, X., Pan, C., Zheng, S., Alhamdi, Y., Sun, B., Shi, Q., Wang, X., Sun, Z., Toh, C., and Wang, G. (2014). Protective effects of carbon monoxide-releasing molecule-2 on the barrier function of intestinal epithelial cells. *PLoS One* **9**, e104032.

Murphy, M. P., and Smith, R. A. (2007). Targeting antioxidants to mitochondria by conjugation to lipophilic cations. *Annu. Rev. Pharmacol. Toxicol.* **47**, 629-656.

National Institute for Occupational Safety and Health (1994). Carbon monoxide: immediately dangerous to life or health (IDLH) concentrations. https://www.cdc.gov/niosh/idlh/630080.html

Ndisang, J. F., Tabien, H. E., and Wang, R. (2004). Carbon monoxide and hypertension. *J. Hypertens.* **22**, 1057-1074.

Nobre, L. S., Jeremias, H., Romao, C. C., and Saraiva, L. M. (2016). Examining the antimicrobial activity and toxicity to animal cells of different types of CO-releasing molecules. *Dalton Trans.* **45**, 1455-1466.

Otterbein, L. E., Bach, F. H., Alam, J., Soares, M., Tao Lu, H., Wysk, M., Davis, R. J., Flavell, R. A., and Choi, A. M. (2000). Carbon monoxide has anti-inflammatory effects involving the mitogen-activated protein kinase pathway. *Nat. Med.* **6**, 422-428.

Otterbein, L. E., Foresti, R., and Motterlini, R. (2016). Heme oxygenase-1 and carbon monoxide in the heart: the balancing act between danger signaling and pro-survival. *Circul. Res.* **118**, 1940-1959.

Palao, E., Slanina, T., Muchova, L., Solomek, T., Vitek, L., and Klan, P. (2016). Transition-metal-free CO-releasing BODIPY derivatives activatable by visible to NIR light as promising bioactive molecules. *J. Am. Chem. Soc.* **138**, 126-133.

Peng, P., Wang, C., Shi, Z., Johns, V. K., Ma, L., Oyer, J., Copik, A., Igarashi, R., and Liao, Y. (2013). Visible-light activatable organic CO-releasing molecules (PhotoCORMs) that simultaneously generate fluorophores. *Org. Biomol. Chem.* **11**, 6671-6674.

Popova, M., Soboleva, T., Arif, A. M., and Berreau, L. M. (2017). Properties of a flavonol-based photoCORM in aqueous buffered solutions: influence of metal ions, surfactants and proteins on visible light-induced CO release. *RSC Advances* **7**, 21997-22007.

Potter, M., Newport, E., and Morten, K. J. (2016). The Warburg effect: 80 years on. *Biochem. Soc. Trans.* **44**, 1499-1505.

Queiroga, C. S., Almeida, A. S., Alves, P. M., Brenner, C., and Vieira, H. L. (2011). Carbon monoxide prevents hepatic mitochondrial membrane permeabilization. *BMC Cell Biol.* **12**, 10.

Queiroga, C. S., Almeida, A. S., and Vieira, H. L. (2012). Carbon monoxide targeting mitochondria. *Biochem. Res. Int.* **2012**, 749845.

Reily, C., Mitchell, T., Chacko, B. K., Benavides, G., Murphy, M. P., and Darley-Usmar, V. (2013). Mitochondrially targeted compounds and their impact on cellular bioenergetics. *Redox Biol.* **1**, 86-93.

Romanski, S., Stamellou, E., Jaraba, J. T., Storz, D., Kramer, B. K., Hafner, M., Amslinger, S., Schmalz, H. G., and Yard, B. A. (2013). Enzyme-triggered CO-releasing molecules (ET-CORMs): evaluation of biological activity in relation to their structure. *Free Radic. Biol. Med.* **65**, 78-88.

Ross, M. F., Prime, T. A., Abakumova, I., James, A. M., Porteous, C. M., Smith, R. A., and Murphy, M. P. (2008). Rapid and extensive uptake and activation of hydrophobic triphenylphosphonium cations within cells. *Biochem. J.* **411**, 633-645.

Sato, K., Balla, J., Otterbein, L., Smith, R. N., Brouard, S., Lin, Y., Csizmadia, E., Sevigny, J., Robson, S. C., Vercellotti, G., *et al.* (2001). Carbon monoxide generated by heme oxygenase-1 suppresses the rejection of mouse-to-rat cardiac transplants. *J. Immunol.* **166**, 4185-4194.

Schatzschneider, U. (2015). Novel lead structures and activation mechanisms for CO-releasing molecules (CORMs). *Br. J. Pharmacol.* **172**, 1638-1650.

Sjostrand, T. (1949). Endogenous formation of carbon monoxide in man. *Nature* **164**, 580.

Smith, R. A., Porteous, C. M., Coulter, C. V., and Murphy, M. P. (1999). Selective targeting of an antioxidant to mitochondria. *Eur. J. Biochem.* **263**, 709-716.

Soboleva, T., Esquer, H. J., Benninghoff, A. D., and Berreau, L. M. (2017). Sense and release: a thiol-responsive flavonol-based photonically driven carbon monoxide-releasing molecule that operates via a multiple-input AND logic gate. *J. Am. Chem. Soc.* **139**, 9435-9438.

Suliman, H. B., Carraway, M. S., Ali, A. S., Reynolds, C. M., Welty-Wolf, K. E., and Piantadosi, C. A. (2007). The CO/HO system reverses inhibition of mitochondrial biogenesis and prevents murine doxorubicin cardiomyopathy. *J. Clin. Invest.* **117**, 3730-3741.

Suliman, H. B., and Piantadosi, C. A. (2014). Mitochondrial biogenesis: regulation by endogenous gases during inflammation and organ stress. *Curr. Pharm. Des.* **20**, 5653-5662.

Suliman, H. B., and Piantadosi, C. A. (2016). Mitochondrial quality control as a therapeutic target. *Pharmacol. Rev.* **68**, 20-48.

Sun, H. J., Xu, D. Y., Sun, Y. X., Xue, T., Zhang, C. X., Zhang, Z. X., Lin, W., and Li, K. X. (2017). CO-releasing molecules-2 attenuates ox-LDL-induced injury in HUVECs by ameliorating mitochondrial function and inhibiting Wnt/beta-catenin pathway. *Biochem. Biophys. Res. Commun.* **490**, 629-635.

Takagi, T., Naito, Y., Uchiyama, K., Suzuki, T., Hirata, I., Mizushima, K., Tsuboi, H., Hayashi, N., Handa, O., Ishikawa, T., *et al.* (2011). Carbon monoxide liberated from carbon monoxide-releasing molecule exerts an anti-inflammatory effect on dextran sulfate sodium-induced colitis in mice. *Dig. Dis. Sci.* **56**, 1663-1671.

Tenhunen, R., Marver, H. S., and Schmid, R. (1968). The enzymatic conversion of heme to bilirubin by microsomal heme oxygenase. *Proc. Natl. Acad. Sci. USA* **61**, 748-755.

Tolosa, L., Donato, M. T., and Gomez-Lechon, M. J. (2015). General cytotoxicity assessment by means of the MTT assay. *Methods Mol. Biol.* **1250**, 333-348.

Trnka, J., Elkalaf, M., and Anděl, M. (2015). Lipophilic triphenylphosphonium cations inhibit mitochondrial electron transport chain and induce mitochondrial proton leak. *PLoS One* **10**, 1-14.

Vadori, M., Seveso, M., Besenzon, F., Bosio, E., Tognato, E., Fante, F., Boldrin, M., Gavasso, S., Ravarotto, L., Mann, B. E., *et al.* (2009). In vitro and in vivo effects of the carbon monoxide-releasing molecule, CORM-3, in the xenogeneic pig-to-primate context. *Xenotransplantation* **16**, 99-114.

Vummaleti, S. V., Branduardi, D., Masetti, M., De Vivo, M., Motterlini, R., and Cavalli, A. (2012). Theoretical insights into the mechanism of carbon monoxide (CO) release from CO-releasing molecules. *Chemistry (Easton)* **18**, 9267-9275.

Wang, D., Viennois, E., Ji, K., Damera, K., Draganov, A., Zheng, Y., Dai, C., Merlin, D., and Wang, B. (2014). A click-and-release approach to CO prodrugs. *Chem. Commun. (Camb.)* **50**, 15890-15893.

Wang, P., Yao, L., Zhou, L. L., Liu, Y. S., Chen, M. D., Wu, H. D., Chang, R. M., Li, Y., Zhou, M. G., Fang, X. S., *et al.* (2016). Carbon monoxide improves neurologic outcomes by mitochondrial biogenesis after global cerebral ischemia induced by cardiac arrest in rats. *Int. J. Biol. Sci.* **12**, 1000-1009.

Willems, P. H., Rossignol, R., Dieteren, C. E., Murphy, M. P., and Koopman, W. J. (2015). Redox homeostasis and mitochondrial dynamics. *Cell Metab.* **22**, 207-218.

Wright, M. A., and Wright, J. A. (2016). PhotoCORMs: CO release moves into the visible. *Dalton Trans.* **45**, 6801-6811.

Xu, J. S., Zeng, F., Wu, H., and Wu, S. Z. (2015). A mitochondrial-targeting and NO-based anticancer nanosystem with enhanced photo-controllability and low dark-toxicity. *J Mater. Chem. B* **3**, 4904-4912.

Yang, Y. C., Huang, Y. T., Hsieh, C. W., Yang, P. M., and Wung, B. S. (2014). Carbon monoxide induces heme oxygenase-1 to modulate STAT3 activation in endothelial cells via S-glutathionylation. *PLoS One* **9**, e100677.

Zerin, T., Kim, Y. S., Hong, S. Y., and Song, H. Y. (2013). Quercetin reduces oxidative damage induced by paraquat via modulating expression of antioxidant genes in A549 cells. *J. Appl. Toxicol.* **33**, 1460-1467.

Zielonka, J., Joseph, J., Sikora, A., Hardy, M., Ouari, O., Vasquez-Vivar, J., Cheng, G., Lopez, M., and Kalyanaraman, B. (2017). Mitochondria-targeted triphenylphosphonium-based compounds: syntheses, mechanisms of action, and therapeutic and diagnostic applications. *Chem. Rev.* **117**, 10043-10120.

Zuckerbraun, B. S., Chin, B. Y., Bilban, M., d'Avila, J. C., Rao, J., Billiar, T. R., and Otterbein, L. E. (2007). Carbon monoxide signals via inhibition of cytochrome c oxidase and generation of mitochondrial reactive oxygen species. *FASEB J.* **21**, 1099-1106.

APPENDICES

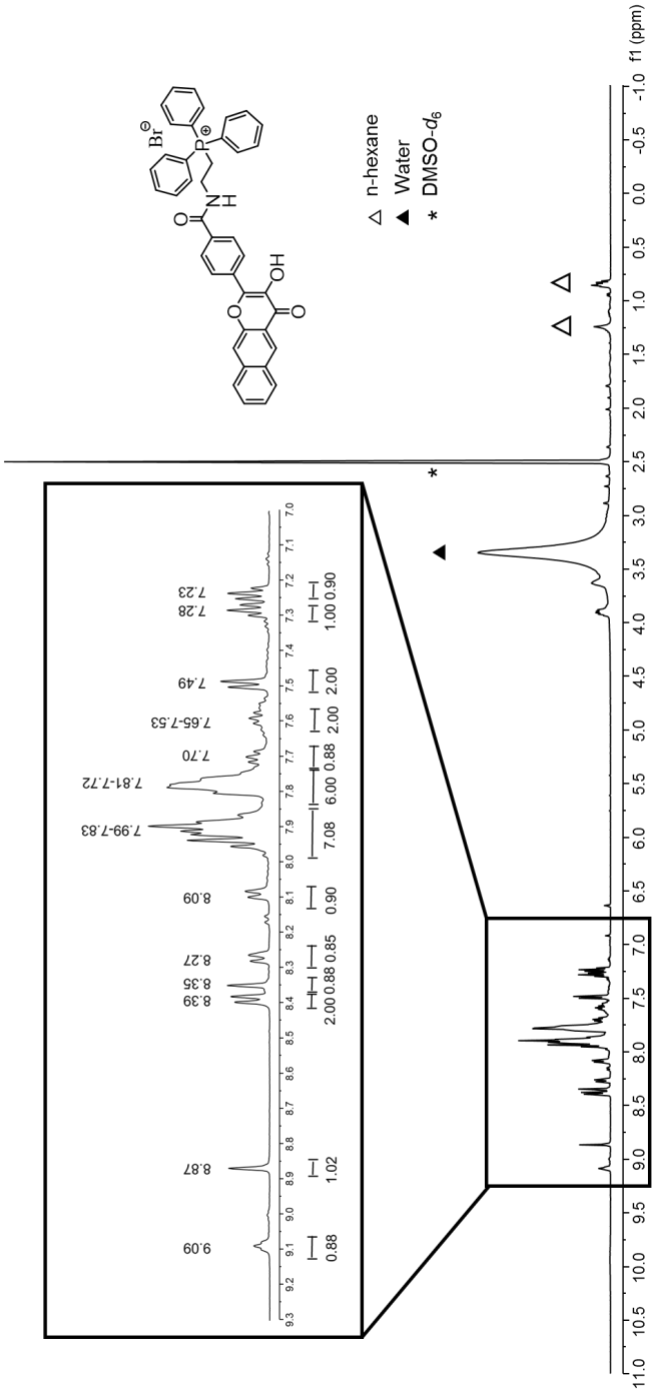

Figure A1. ^{1}H NMR of Mito-Flav-C2 in DMSO-d_6. Data shown with permission of collaborators Tatiana Soboleva and Lisa Berreau, Utah State University.

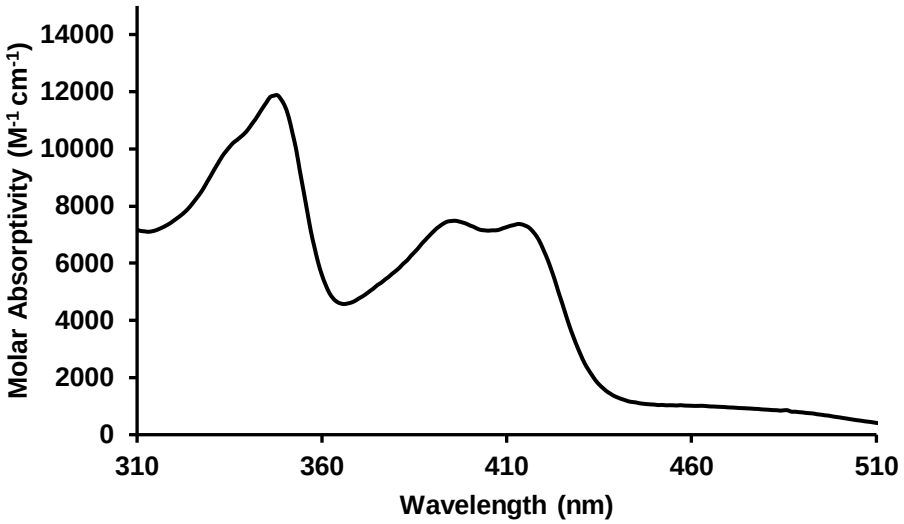

Figure A2. Absorption spectrum of Mito-Flav-C2 in CH_3CN:DMSO (10:1). Data shown with permission of collaborators Tatiana Soboleva and Lisa Berreau, Utah State University.

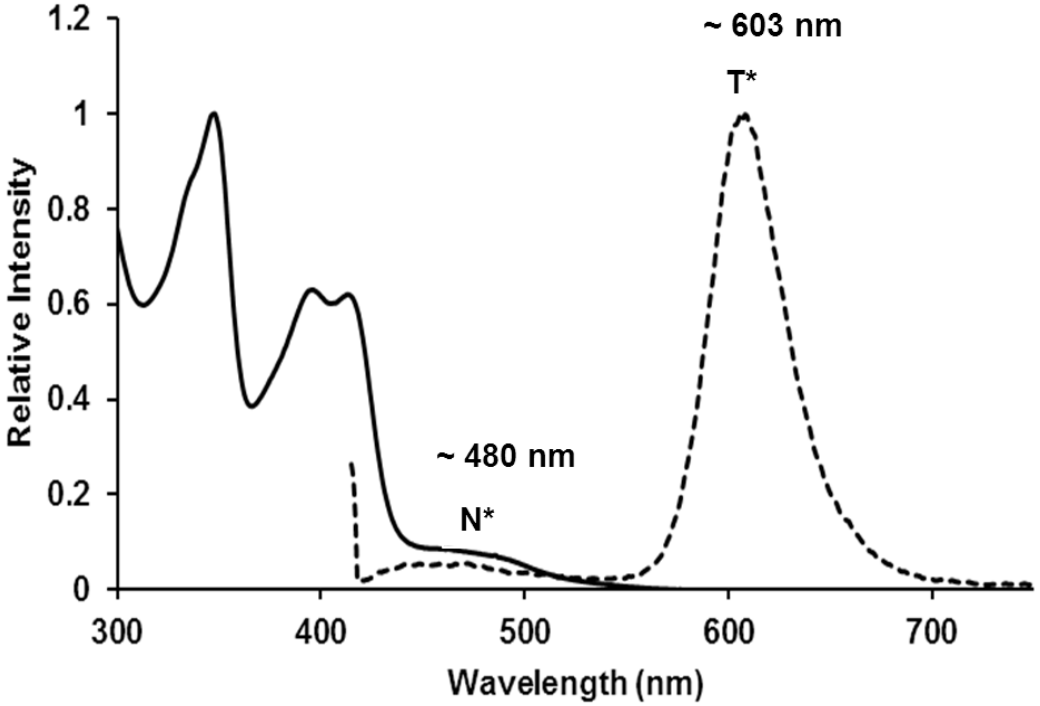

Figure A3. Overlay of normalized lowest energy absorption features of Mito-Flav-C2 with the emission spectrum in CH_3CN:DMSO (10:1). Emission features at ~480 nm and ~603 nm represent normal (N*) and tautomeric (T*) excited forms of the flavonol core respectively. Data shown with permission of collaborators Tatiana Soboleva and Lisa Berreau, Utah State University.

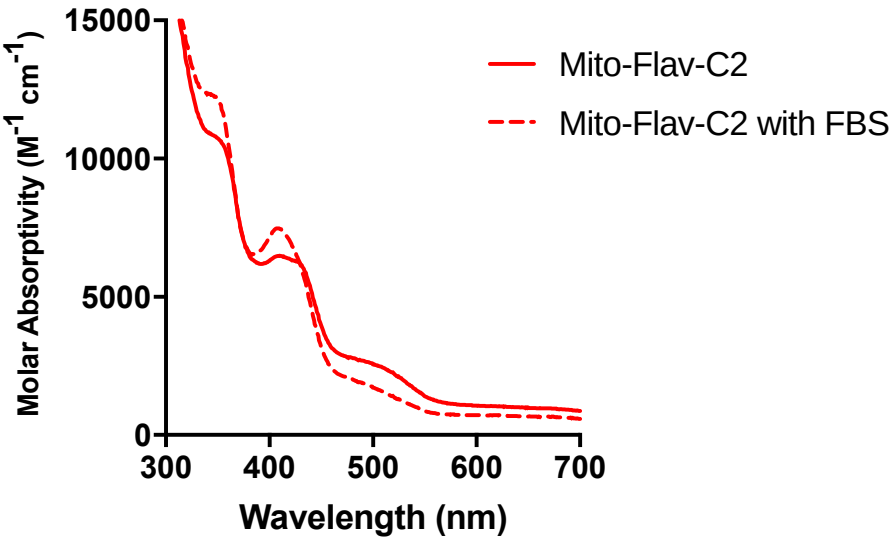

Figure A4. Absorption spectrum of Mito-Flav-C2 in DMEM F12 cell culture media with and without 10% (v/v) FBS. Data shown with permission of collaborators Tatiana Soboleva and Lisa Berreau, Utah State University.

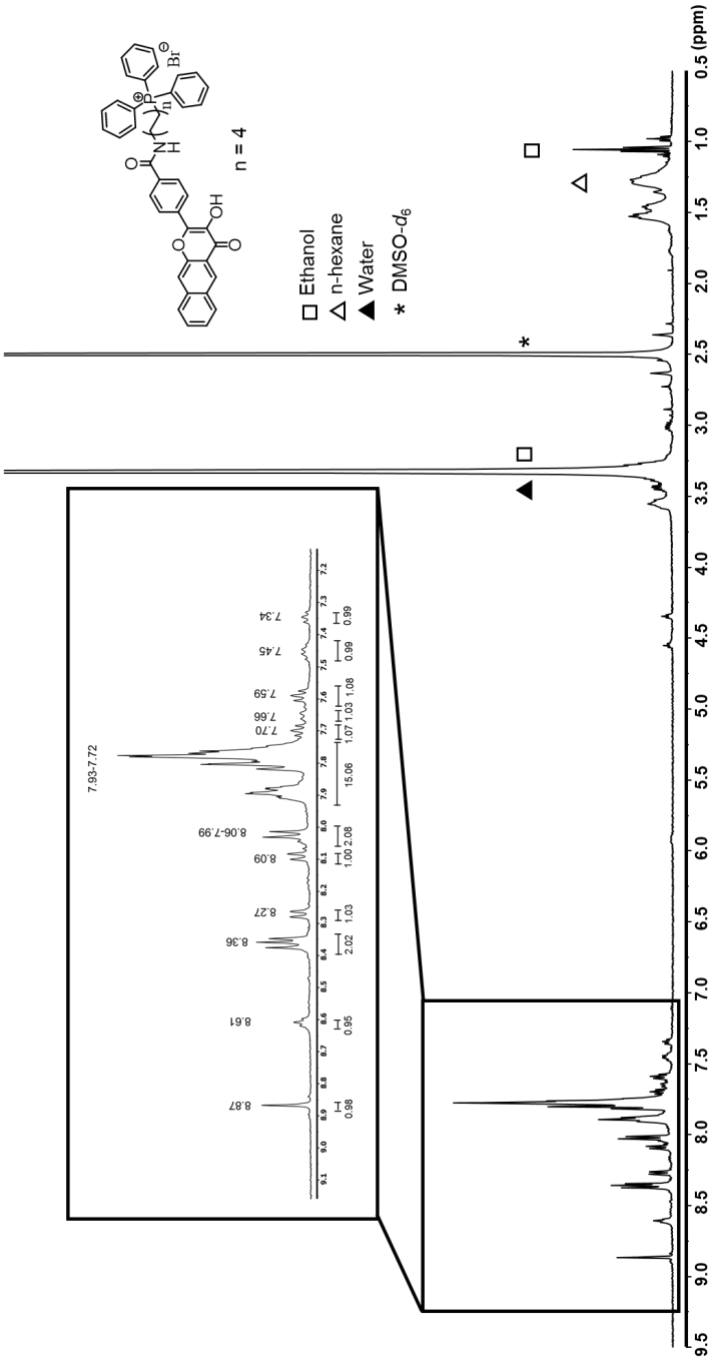

Figure A5. ^{1}H NMR of Mito-Flav-C8 in DMSO-d_6. Data shown with permission of collaborators Tatiana Soboleva and Lisa Berreau, Utah State University.

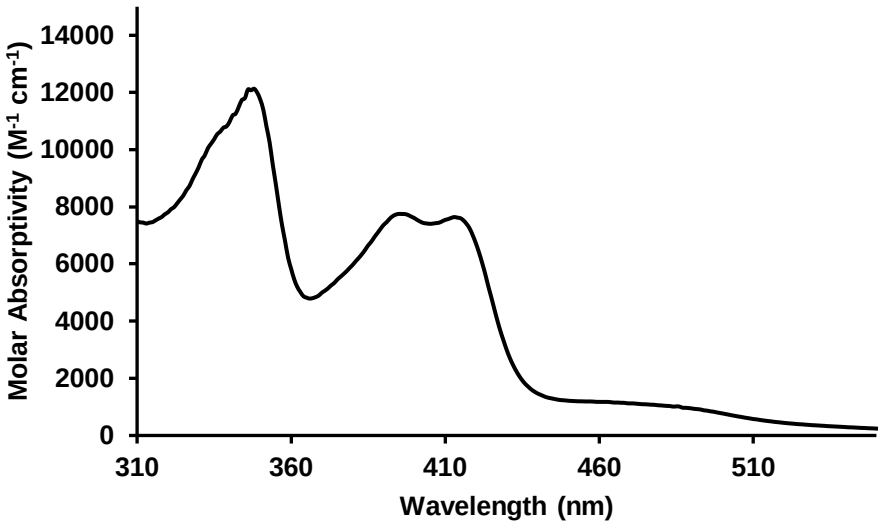

Figure A6. Absorption spectrum of Mito-Flav-C8 in CH_3CN:DMSO (10:1). Data shown with permission of collaborators Tatiana Soboleva and Lisa Berreau, Utah State University.

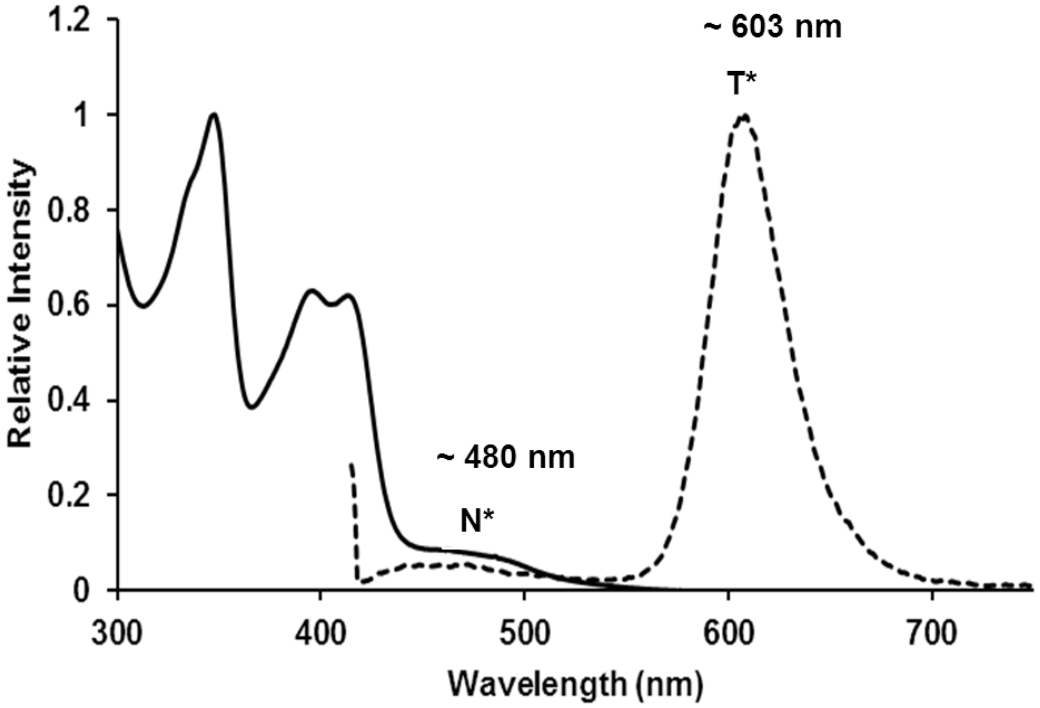

Figure A7. Overlay of normalized lowest energy absorption feature of Mito-Flav-C8 with its emission spectrum in CH_3CN:DMSO (10:1). Emission features at ~480 nm and ~603 nm represent normal (N*) and tautomeric (T*) excited states of the flavonol core respectively. Data shown with permission of collaborators Tatiana Soboleva and Lisa Berreau, Utah State University.

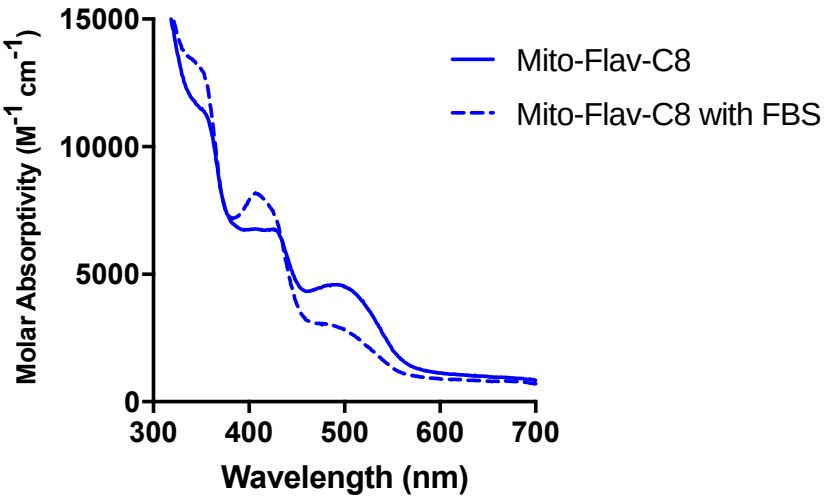

Figure A8. Absorption spectrum of Mito-Flav-C8 in DMEM F12 cell culture media with and without 10% (v/v) FBS. Data shown with permission of collaborators Tatiana Soboleva and Lisa Berreau, Utah State University.

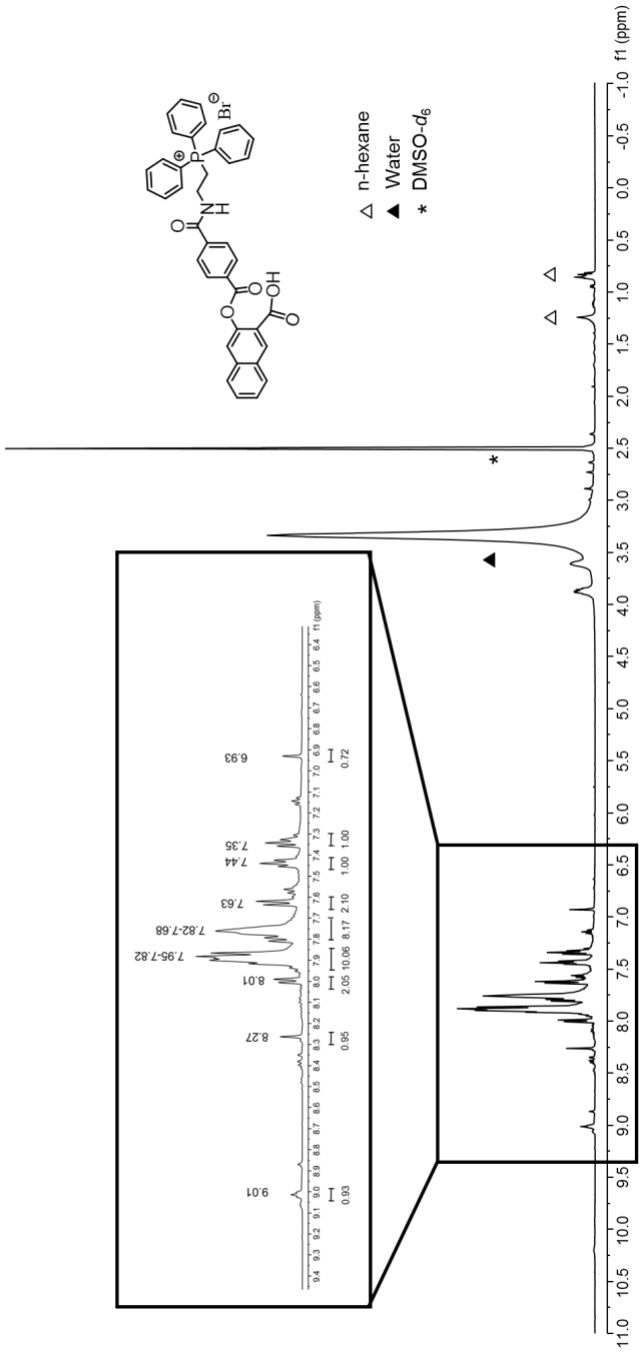

Figure A9. ^{1}H NMR of Irr-Mito-Flav-C2 in DMSO-d_6 illuminated at 419 nm for 24 h. Data shown with permission of collaborators Tatiana Soboleva and Lisa Berreau, Utah State University.

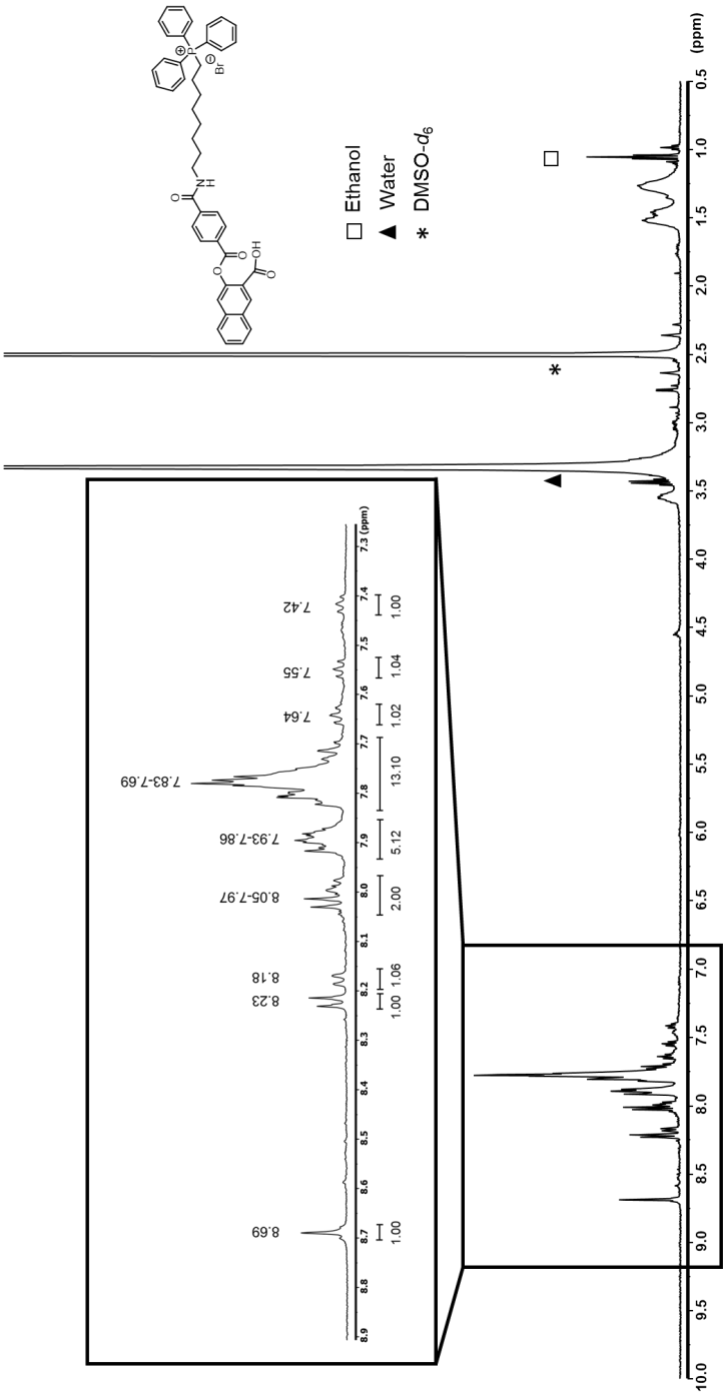

Figure A10. ^{1}H NMR of Irr-Mito-Flav-C8 in DMSO-d_6 illuminated at 419 nm for 24 h. Data shown with permission of collaborators Tatiana Soboleva and Lisa Berreau, Utah State University.

Table A1. Summary of Confocal Microscopy Experiments with Flav-1, Mito-Flav-C2 and Mito-Flav-C8 in A549 and HUVEC Cell Lines.

							Fluorescence signal for CORM (%)						
Cell line	CORM	Conc. (μM)	Time (h)	Fields of view	Cells imaged	Positive cells (%)	S	MS	M	MW	W	F	N
A549	Flav-1	25	1	3	21	0	0	0	0	0	0	0	100
A549	Flav-1	50	1	4	42	0	0	0	0	0	0	0	100
A549	Flav-1	75	1	4	43	0	0	0	0	0	0	0	100
A549	Flav-1	75	4	3	33	0	0	0	0	0	0	0	100
A549	Flav-1	100	4	7	80	0	0	0	0	0	0	0	100
A549	Flav-1	100	4	3	51	0	0	0	0	0	0	0	100
A549	C2	25	4	6	79	62	0	42	0	0	20	0	38
A549	C2	50	4	6	56	100	0	0	16	0	32	52	0
A549	C2	75	4	6	61	59	0	0	0	28	31	41	0
A549	C2	75	4	8	71	96	23	58	15	0	0	0	4
A549	C2	100	4	6	123	100	35	24	41	0	0	0	0
A549	C2	100	4	10	163	100	48	44	9	0	0	0	0
A549	C8	100	4	5	49	100	61	39	0	0	0	0	0
A549	C8	100	4	11	56	100	0	0	100	0	0	0	0
A549	C8 (EtOH)	100	4	6	118	100	0	0	48	52	0	0	0
A549	C8 (EtOH)	100	4	5	51	94	0	0	12	22	61	0	6
A549	C8 (EtOH)	100	4	7	42	67	0	0	67	0	0	0	33
HUVEC	Flav-1	100	1	5	91	97	0	0	0	75	22	0	3
HUVEC	Flav-1	100	4	12	64	100	0	0	0	0	0	100	0
HUVEC	Flav-1	100	4	10	55	49	0	0	0	0	0	49	51
HUVEC	C2	100	4	13	65	97	26	26	45	0	0	0	3

Table A1. Summary of Confocal Microscopy Experiments with Flav-1, Mito-Flav-C2 and Mito-Flav-C8 in A549 and HUVEC Cell Lines.

							Fluorescence signal for CORM (%)						
Cell line	CORM	Conc. (μM)	Time (h)	Fields of view	Cells imaged	Positive cells (%)	S	MS	M	MW	W	F	N
HUVEC	C2	100	4	8	43	100	70	12	19	0	0	0	0
HUVEC	C8	100	4	12	31	100	0	19	58	19	3	0	0
HUVEC	C8	100	4	8	46	100	0	67	17	0	15	0	0
HUVEC	C8	100	4	7	51	100	0	0	69	25	6	0	0
HUVEC	C8 (EtOH)	100	4	5	18	89	0	0	44	44	0	0	11

The intensity of the fluorescence signal was scored qualitatively as follows: S, strong; MS, moderately strong; M, moderate; MW, moderately weak; W, weak; F, faint; N, none.

UtahState University

July 5, 2017

Lisa M. Berreau and Tatiana Soboleva
Department of Chemistry and Biochemistry
0300 Old Main Hill
Logan, Utah 84322

Dear Dr. Berreau and Ms. Soboleva,

I am in the process of preparing my thesis in the Department of Animal, Dairy and Veterinary Sciences at Utah State University. I hope to complete my degree program in Toxicology. I am requesting your permission to include the attached material as shown. I will include acknowledgments to your work with a specific reference in each figure legend, as indicated: "Data with permission of collaborators Tatiana Soboleva and Lisa Berreau, Utah State University." Please indicate your approval of this request by signing below in the space provided, attaching any other form or instruction necessary to confirm permission. Thank you for your assistance and collaboration.

Best regards,

Hector Esquer

We hereby give permission to Hector Esquer to reprint the following material in his thesis.

Figure 6. Absorption spectrum of Flav-1
Figure 7. Emission spectra of Flav-1
Figure 12. Emission intensity spectra for Flav-1, Mito-Flav-C2, and Mito-Flav-C8
Figure A1. NMR spectra of Mito-Flav-C2
Figure A2. Absorption spectrum for Mito-Flav-C2 in CH_3CN:DMSO
Figure A3. Overlay of normalized lowest energy absorption feature of Mito-Flav-C2 with the emission spectrum in CH_3CN:DMSO
Figure A4. Absorption spectrum of Mito-Flav-C2 in DMEM F12 cell culture media with and without 10% (v/v) FBS
Figure A5. NMR spectra of Mito-Flav-C8
Figure A6. Absorption spectrum for Mito-Flav-C8 in CH_3CN:DMSO
Figure A7. Overlay of normalized lowest energy absorption feature of Mito-Flav-C2 with the emission spectrum in CH_3CN:DMSO
Figure A8. Absorption spectrum of Mito-Flav-C8 in DMEM F12 cell culture media with and without 10% (v/v) FBS